Electrochemical Behavior and Shape Evolution of Structured Pd Nanoparticles in Alkaline Media Influence of Electrochemically Absorbed Hydrogen

Sho Fujita, Stève Baranton, Christophe Coutanceau, Gregory Jerkiewicz

Electrochemical Behavior and Shape Evolution of Structured Pd Nanoparticles in Alkaline Media – Influence of Electrochemically Absorbed Hydrogen

Journal:	*Langmuir*
Manuscript ID	la-2023-01636v.R1
Manuscript Type:	Article
Date Submitted by the Author:	18-Sep-2023
Complete List of Authors:	Fujita, Sho; Queen's University, Chemistry Baranton, Stève; Universite de Poitiers, Equipe électrocatalyse Coutanceau, Christophe; Universite de Poitiers, IC2MP UMR CNRS n° 7285 Jerkiewicz, Gregory; Queen's University, Chemistry

Electrochemical Behavior and Shape Evolution of Structured Pd Nanoparticles in Alkaline Media – Influence of Electrochemically Absorbed Hydrogen

Sho Fujita[a], Stève Baranton[b], Christophe Coutanceau[b], and Gregory Jerkiewicz[a]**

[a] Department of Chemistry, Queen's University, 90 Bader Lane, Kingston, Ontario K7L 3N6, Canada

[b] IC2MP, UMR CNRS 7285, Université de Poitiers, 4 rue Michel Brunet, TSA 51106, 86073, Poitiers Cedex 9, France

ABSTRACT

We report on the electrochemical behavior and shape evolution of Pd nanocubes (Pd NCs) and Pd nanooctahedrons (Pd NOs) with an average size of 9.8 nm and 6.9 nm, respectively, in aqueous alkaline medium in the potential range of the underpotential deposition of H (UPD H) and H absorption. While the Pd NCs and Pd NOs remain stable in the potential region of the UPD H, H absorption and desorption induce structural changes to the Pd NPs, as indicated by the results of electrochemical measurements and identical-location transmission electron microscopy (IL-TEM) analyses. Because both Pd NCs and Pd NOs are known to be stable in the potential region of H absorption and desorption in acidic medium and maintain their structure, the irreversible structural changes are attributed to their interfacial interaction with the aqueous alkaline medium. In the alkaline medium, the nanoparticle surface/electrolyte interfacial structure plays an essential role in the mechanism of H desorption that is observed at higher potentials than in the acidic medium. Hydrogen desorption is substantially hindered due to the structure of water network adjacent to the Pd nanoparticles or the interaction between hydrated cations and adsorbed OH on the nanoparticle surface, resulting in the trapping of a small amount of H (incomplete H desorption). It is proposed that H trapping and associated structural strain lead to deformation of the Pd nanoparticles and loss of their initial structure.

GRAPHICAL ABSTRACT

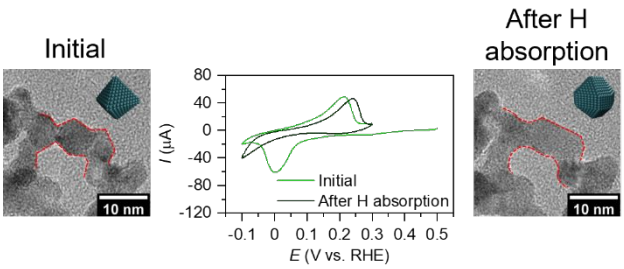

KEYWORDS

Palladium nanoparticles, H electro-absorption, H loading, aqueous alkaline media, identical location transmission electron microscopy, nanoparticle stability, nanoparticle structure

INTRODUCTION

About 150 years ago, palladium (Pd) materials were found to absorb a large amount of H[1] and since then have found various applications, such as hydrogen storage,[2–4] hydrogen detection,[5,6] hydrogen purification,[7] as well as electrode materials (electrocatalysts) for electrocatalytic hydrogenation.[8–11] The H absorption in Pd materials occurs under gas-phase conditions in the presence of H_2(g) or aqueous electrochemical conditions in the presence of H^+ and H_2O (acidic media) or OH^- and H_2O (alkaline media). In both gas-phase and electrochemical conditions, Pd materials develop two different H-containing phases, namely the α and β phases, depending on the amount of the absorbed H (H_{abs}). The α phase is a solid-state solution of Pd with a small amount of H_{abs} (H_{abs}/Pd ≤ 0.03), while the β phase is a metal-hydride with a large amount of H_{abs} (H_{abs}/Pd ≥ 0.6) having its unique crystallographic structure and lattice parameter that are different from those of Pd.

When analyzing the mechanism of H absorption, one needs to consider the unique environmental difference between the metal/gas and metal/liquid interfaces (Figure 1).[12] At the metal/gas interface, the hydrogen molecule (H_2) is dissociated at the surface of the metal and produces adsorbed H (H_{ads}).

$$H_2(g) \leftrightarrow 2H^* \quad (1)$$

$$2M + 2H^* \leftrightarrow 2M\text{–}H_{ads} \quad (2)$$

where M is the active site of the metal, and H^* is the short-lived energetically rich H that eventually forms a chemical bond with a metal atom. Following its formation, the H_{ads} species undergoes transfer to the sub-surface region of the metal and becomes sub-surface H (H_{ss}), and eventually diffuses from the sub-surface site into the bulk of the metal to become absorbed H (H_{abs}).[13] In the case of the metal/liquid interface, the H_{ads} species is generated from H^+ or H_2O along with the charge-transfer process.

$$M + H^+(aq) + e^- \leftrightarrow M\text{–}H_{ads} \quad \text{(acidic media)} \quad (3)$$

$$M + H_2O + e^- \leftrightarrow M\text{–}H_{ads} + OH^-(aq) \quad \text{(alkaline media)} \quad (4)$$

Similarly to the gas phase, the H_{ads} species undergoes transfer beneath the first surface layer and becomes H_{ss}, and subsequently becomes H_{abs} upon its diffusion into the bulk of the metal host. The host metal surface experiences interactions with the components in electrolyte solution (*e.g.*, water molecules, anions, and cations), which can give rise to the formation of new metallic structures (*e.g.,* defects, such as steps, kinks, voids, cracks) and even surface compounds. The H electro-adsorption is known to take place at potentials higher than the onset potential of the

hydrogen evolution reaction (HER) and below it; the respective processes are known as the underpotential deposition of H (UPD H) and the overpotential deposition of H (OPD H).[14] It is important to note that the UPD H is characteristic of only the platinum group metals (PGMs), such as Pt, Ir, Rh, including Pd, while the OPD H takes place on all electrode materials at which the HER occurs. In the case of other transition metals such as for example Ni, the adsorption of H_{UPD} is not observed because the formation of an oxygen-containing surface compound (α-$Ni(OH)_2$) is thermodynamically favorable.[12]

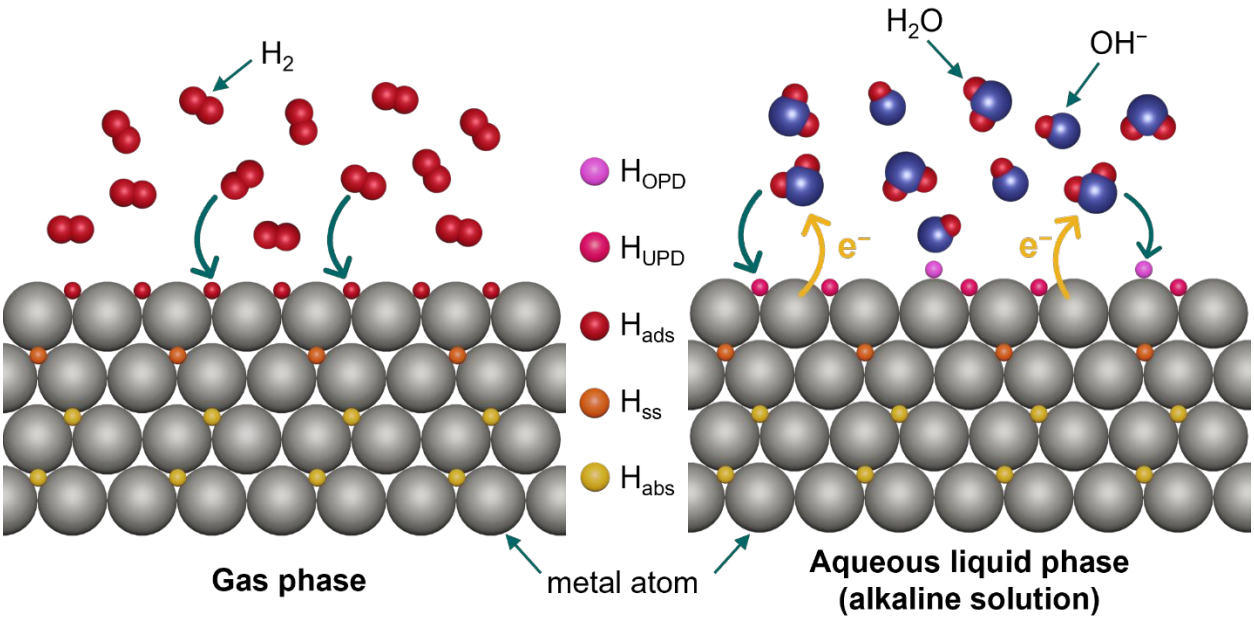

Figure 1. Visual representation of the steps involved in H absorption under gas-phase (H_2(g) at a low pressure) and electrochemical conditions (in aqueous alkaline solution).

Among all PGMs, Pd is unique in the sense that in addition to adsorbing H it can also absorb it, and the electrochemical H adsorption and absorption have been examined using a wide range of Pd electrodes (*e.g.,* thin layers on a non-absorbing substrate,[15–19] nanoparticles,[19–23] single-crystals[24,25]). In the case of bulk Pd in aqueous acidic media, it is impossible to study the UPD H using cyclic voltammetry (CV) because the H absorption takes place already in the potential range of the UPD H and the current density due to H absorption is greater than that due to the UPD H; the CV features associated with these two processes overlap.[26] By using very thin Pd layers deposited on polycrystalline or monocrystalline Au substrates, the feature of UPD H can be clearly observed.[15,17,27,28] If the deposited film is thin enough and the Au substrate monocrystalline in nature, then the observed electrochemical features are characteristic of the surface orientation of the Au substrate, and as a result, the CV profiles resemble those typical of Pd single crystals. The use of Pd NPs is also effective in investigating the UPD H and H absorption because the large surface area-to-volume ratio results in a clear separation of the regions ascribed to the UPD H and H absorption in CV profiles.[22,23] Elsewhere, it was demonstrated that Pd NPs can absorbed more H as compared by bulk Pd materials by tuning their shape and thus the surface structure.[23,29]

The unique structures of the shape-controlled Pd NPs can be created by the use of suitable stabilizers and capping reagents in their synthesis, but it is important to emphasize that the cleanliness of the NPs is critical for their use in electrochemical applications as the stabilizers or capping reagents can remain at the NP surface and reduces the number of active sites.[30] In the case of thoroughly cleaned shape-controlled Pd NPs, the CV profiles in acidic aqueous electrolyte solution reveal distinct features associated with the UPD H, H absorption/desorption, and HER.[23] In the case of the octahedral Pd NPs, the amount of H_{abs} was significantly larger (*ca.* 50% larger) than in the case of bulk Pd materials; thus, the octahedral Pd NPs are considered to be a promising anode nanomaterial for miniaturized nickel-metal hydride (Ni-MH) batteries.[29] Because Ni-MH batteries are alkaline batteries typically employing a highly concentrated aqueous solution of KOH, it is important to investigate the electrochemical behavior of shaped-controlled Pd NPs in this electrolyte solution but to the best of our understanding this knowledge does not exist at the present time.

In this study, we report on the electrochemical behaviour of the shape-controlled Pd NPs, namely Pd nanocubes (Pd NCs) and Pd nanooctahedrons (Pd NOs), in aqueous alkaline medium in the potential regions of H adsorption and H absorption. The average size of the Pd NCs and NOs is

9.8 nm and 6.9 nm, respectively, and is in agreement with the size of the shape-controlled Pd NPs employed in our previous research focused on their behaviour in aqueous acidic media.[23,29] The stability of the shape-controlled Pd NPs was investigated by carefully executed CV and identical-location transmission electron microscopy (IL-TEM) measurements. The changes in the surface properties of the Pd NCs and Pd NOs were also assessed prior to and after the stability tests by conducting CO stripping experiments. The results reveal modification of the shape of both the Pd NCs and Pd NOs in response to the electrochemical H adsorption and absorption, as well as desorption in the aqueous alkaline medium. Such surface structure modification of the shape-controlled Pd NPs was not observed in the case of aqueous acidic medium,[23,29] and therefore this unique behaviour is attributed to the structure of the NP surface-electrolyte interface, which impacts the H absorption and adsorption.

EXPERIMENTAL

Synthesis of Shape-controlled Pd NPs

Pd NCs and Pd NOs were synthesized by a chemical reduction method using an aqueous solution with polyvinylpyrrolidone (PVP) and different capping reagents.[29,31] For the preparation of the Pd

NCs, a Pd precursor solution was prepared by dissolving 0.062 g of K_2PdCl_4 (99.99%, Alfa Aesar), 0.300 g of KBr (99.95%, Sigma-Aldrich), and 0.100 g of PVP (MW ≈ 55000, Sigma-Aldrich) in 7.00 mL of ultra-high purity (UHP) water (MilliQ, Millipore, 18.2 MΩ cm). The mixture was heated up to 80 ˚C in a heating water bath and maintained at this temperature for 30 minutes. 0.060 g of ascorbic acid (Reagent Grade, Sigma-Aldrich) was dissolved in 4.00 mL of UHP water, and the reducing solution was mixed with the Pd NCs precursor solution (after 30 minutes of heating at 80 ˚C). The mixture was allowed to rest for 3 hours at 80 ˚C yielding the desired Pd NCs. The synthesis of Pd NOs follows the same procedure by using different Pd precursor and reducing solutions. The precursor solution was prepared by dissolving 0.062 g of K_2PdCl_4 and 0.100 g of PVP in 8.00 mL of water-ethanol mixture (3:1 v/v). To prepare the reducing solution, 0.180 g of citric acid (reagent grade, Sigma-Aldrich) was dissolved in 3.00 mL of a water-ethanol mixture (2:1 v/v). The synthesized Pd NCs and Pd NOs were cleaned to achieve complete removal of PVP and each capping reagent by repetitive soaking first with NaOH (Reagent Grade, Sigma-Aldrich) aqueous solution at least three times and then with UHP water also at least three times. The cleanliness of the Pd NCs and Pd NOs was verified by conducting CV measurements in 0.50 M aqueous H_2SO_4 (Suprapur, Merck) solution (the characteristics of the CV profiles are known to be

unique to the shape of the Pd NPs and cleanliness of the system; the expected CV features are not observed if there are impurities either in the electrolyte solution or on the surface of the NPs).

Electrochemical Measurements

The electrochemical measurements were conducted using a three-electrode electrochemical cell at room temperature (T = 293 ± 1 K). The working electrode (WE) was comprised of the shape-controlled Pd NPs deposited on a gold disc (99.95%, Alfa Aesar) with a diameter of 3.00 mm that acted as a substrate. The surface of the gold disc was polished to a mirror-like finish before each experiment and 3.00 μL of a Pd aqueous suspension was dropcast on it. The total amount of the shape-controlled Pd NPs was *ca.* 14 μg after drying with N_2(g) (99.999%, Praxair). A glassy carbon plate and a reversible hydrogen electrode (RHE) were used as counter and reference electrodes (CE, RE), respectively. To examine the shape-controlled Pd NPs in an acidic or alkaline aqueous medium, CV measurements were performed in 0.50 M aqueous H_2SO_4, 0.10 M aqueous $HClO_4$ (OmniTrace, Merck), and 0.10 M aqueous NaOH solutions. The alkaline medium was prepared from sodium hydroxide monohydrate (NaOH · H_2O, 99.996%, Alfa Aesar). The electrolyte was degassed by bubbling N_2(g) for 1 hour prior to each experiment and N_2(g) was passed above the electrolyte solution during the measurements. All the electrochemical

measurements were carried out with an Autolab model PGSTAT302 potentiostat/galvanostat (Metrohm) controlled using proprietary software (NOVA 2.1).

CO stripping experiments were also conducted for the shape-controlled Pd NPs in the 0.10 M aqueous NaOH solution using the same electrochemical measurement setups. Prior to the measurement, the electrolyte solution was saturated with CO and a constant potential of $E = 0.10$ V was applied for 5 min to form a CO adsorbed layer (CO_{ads}) on the surface of the Pd NPs. Subsequently, the dissolved CO was removed by purging the electrolyte with N_2(g) for 30 min with the potential maintained at $E = 0.10$ V, followed by a potential sweep from $E = 0.10$ V to $E = 1.00$ V at $s = 5.00$ mV s^{-1} to achieve the CO stripping.

The electrochemical behaviours of the Pd NCs and Pd NOs, namely their stability upon repetitive potential cycling in the region of electrochemical H adsorption, absorption, and desorption, was one of the main objectives of this research. The potential cycling (CV measurements) was conducted in the presence of N_2(g) between $E = -0.10$ V and $E = 0.35$ V at $s = 1.00$ mV s^{-1} in the case of the Pd NCs and between $E = -0.10$ V and $E = 0.30$ V in the case of the Pd NOs. Following the repetitive potential cycling, CV profiles for the Pd NPs obtained prior to this treatment were

compared to those obtained afterwards. The results are denoted as *initial* and *after H absorption* in figures, respectively.

Physicochemical Characterization

Transmission electron microscopy (TEM, Talos F200i instrument, Thermo Fisher Scientific) was employed to characterize the structure and size of the shape-controlled Pd NPs deposited on a 200-mesh gold grid with markers. From the TEM images, the length of the longer edge of the Pd NCs and the tip-to-tip length of the Pd NOs were examined to determine the mean sizes of the NPs. In each instance, the distribution of the particle sizes was assessed by measuring 300 particles. The identical-location transmission electron microscopy (IL-TEM) analyses were conducted as follows: (i) the shape-controlled Pd NPs were deposited on a gold grid and subject to a TEM analysis; (ii) the TEM sample was employed as a working electrode in a three-electrode electrochemical cell, and CV experiments were conducted in the presence of N_2(g) between E = −0.10 V and E = 0.35 V (Pd NCs) or E = 0.30 V (Pd NOs) at room temperature and s = 1.00 mV s^{-1}; (iii) the TEM sample was rinsed with UHP water, dried under gentle N_2(g) stream, and a TEM analysis was conducted to verify the structural changes of the Pd NPs after the CV measurements.

RESULTS AND DISCUSSION

Electrochemical Behavior of the Pd Nanoparticles during the UPD and H Absorption and Desorption. Figure 2 presents CV profiles obtained for the Pd NCs and Pd NOs (freshly prepared, thus being in an initial state) in 0.50 M aqueous H_2SO_4 (the upper graphs) and 0.10 M aqueous NaOH solution (the lower graphs) at a potential scan rate of $s = 5.00$ mV s^{-1} and a temperature of $T = 293$ K in the 0.10 – 0.70 V range. In the acidic medium, the CV profiles reveal the following: (i) a flat, featureless double-layer charging region of very low current (I) for both Pd NCs and Pd NOs (0.35 – 0.70 V); (ii) two well-defined cathodic and anodic peaks attributed to the UPD H; the shape of these features depends on the shape of the Pd NPs; and (iii) the current of the peaks at lower potentials is much lower than that of the peaks at higher potentials(Figure 2a,b). These CV characteristics are in good agreement with our previously reported results and indicate that the NPs and the experimental set-up are very clean.[23,29] In the alkaline medium, the behaviour is significantly different and the CV profiles reveals the following: (i) a narrow double-layer charging region with a significant current (0.55 – 0.70 V for the Pd NCs and 0.45 – 0.70 V for the Pd NOs); (ii) in the case of the Pd NCs, two anodic peaks (at $E = 0.35$ V and $E = 0.49$ V) and one cathodic peak ($E = 0.28$ V) attributed to the UPD H; the UPD H occurs in the entire 0.10 – 0.55 V range;

in the case of the Pd NOs, broad waves with weakly pronounced peaks also attributed to the UPD H (0.10 – 0.50 V); these CV characteristics are related to the shape and size of the Pd NPs;[18,32] and (iii) a small reversible feature in the 0.55 – 0.70 V range in the case of the Pd NOs that is assigned to the formation and reduction of a Pd surface oxide (Figure 2c,d).[26,33]

Any eventual application of the shape-controlled Pd NPs (here, Pd NCs and Pd NOs) depends on their stability. Consequently, we examined their behaviour by conducting CV measurements (repetitive potential cycling experiments) in the potential range of the UPD H (Figure 3a,b) and the H absorption and desorption (Figure 3c,d). It is important to mention that our previous findings revealed that the same Pd NPs remained stable upon repetitive potential cycling in aqueous acidic media.[23,29] The CV profiles for the Pd NCs and Pd NOs demonstrate that the current of the cathodic (adsorption of H_{UPD}) and anodic (desorption of H_{UPD}) peaks slightly decreases; the decrease is pronounced the most from the 1st to the 2nd scan and then progresses in small intervals (because the changes are small, only the 1st, 5th, and 10th transients are presented in Figure 3a,b). Since the shape of the CV profiles does not change and the current remains almost the same over the ten transients, it may be concluded that the shape-controlled Pd NPs maintain their original structure. However, the CV profiles for the H absorption and desorption of H_{abs} (Figure 3c,d)

undergo significant changes even within the initial five potential cycles (Figure 3c,d; the first CV transient commences at 0.50 V and covers the potential range of the UPD H and H absorption; the subsequent cycles commence at 0.35 V in the case of the Pd NCs and 0.30 V in the case of the Pd NOs). In the case of both the Pd NCs and Pd NOs, a large cathodic peak at $E = 0.00$ V associated with H absorption is observed in the first cycle and its current significantly decreases from the 1st to the 2nd potential cycle, becomes a small overlapping peak in the 2nd cycles and is not observed anymore in the subsequent cycles. However, there are hardly any changes in the size and shape of the anodic (desorption of H_{abs}) peak, which shifts slightly towards more positive potentials (from $E = 0.26$ V to $E = 0.28$ V in the case of the Pd NCs and from $E = 0.21$ V to $E = 0.24$ V in the case of the Pd NOs) over the five cycles; its current decreases but only slightly. The charge values (Q) corresponding to the amount of H_{abs} were calculated by integrating the anodic peaks on the CV transients for each potential cycle and are presented in Figure 3e,f. It is important to emphasize that it is impossible to determine the amount of H_{abs} based on the cathodic transients because they also contain a contribution from the concurrently occurring hydrogen evolution reaction (HER). In determining the values of Q, it was assumed that the amount of electrochemically absorbed H in the cathodic transient equals to the amount of the desorbed H_{abs} in the anodic one. In the case

of the Pd NCs, the value of Q decreases from 6.44 mC to $Q = 4.53$ mC, thus *ca.* 30% over the five potential cycles. In the case of the Pd NOs, the value of Q decreases from 5.03 mC to 4.27 mC, thus *ca.* 15%. The decrease in the value of Q as the number of potential cycles increases could be attributed to: (i) (electro-)dissolution of the outer layers of the Pd NPs that would decrease their size and, consequently, the amount of H_{abs} that they can host; or/and (ii) structural changes of the Pd NPs. The (electro-)dissolution is unlikely to occur as the applied potentials do not exceed the potential range of the UPD H region and the dissolution of Pd is expected to begin at the potentials higher than $E = 0.70$ V.[26] Thus, the decrease in the value of Q may only be attributed to a shape modification from cubic or octahedral to spherical with a simultaneous decrease in the amount of H_{abs}. Assuming that the number of Pd atoms remains constant in the NPs (we emphasize that there is no Pd loss through (electro-)dissolution), the transition from a cube or an octahedron to a sphere (or a near-sphere) reduces the surface area of the NPs. Because the electrochemical absorption of H proceeds through the surface, the change in the shape of the NPs explains the experimentally observed decrease in the values of Q.

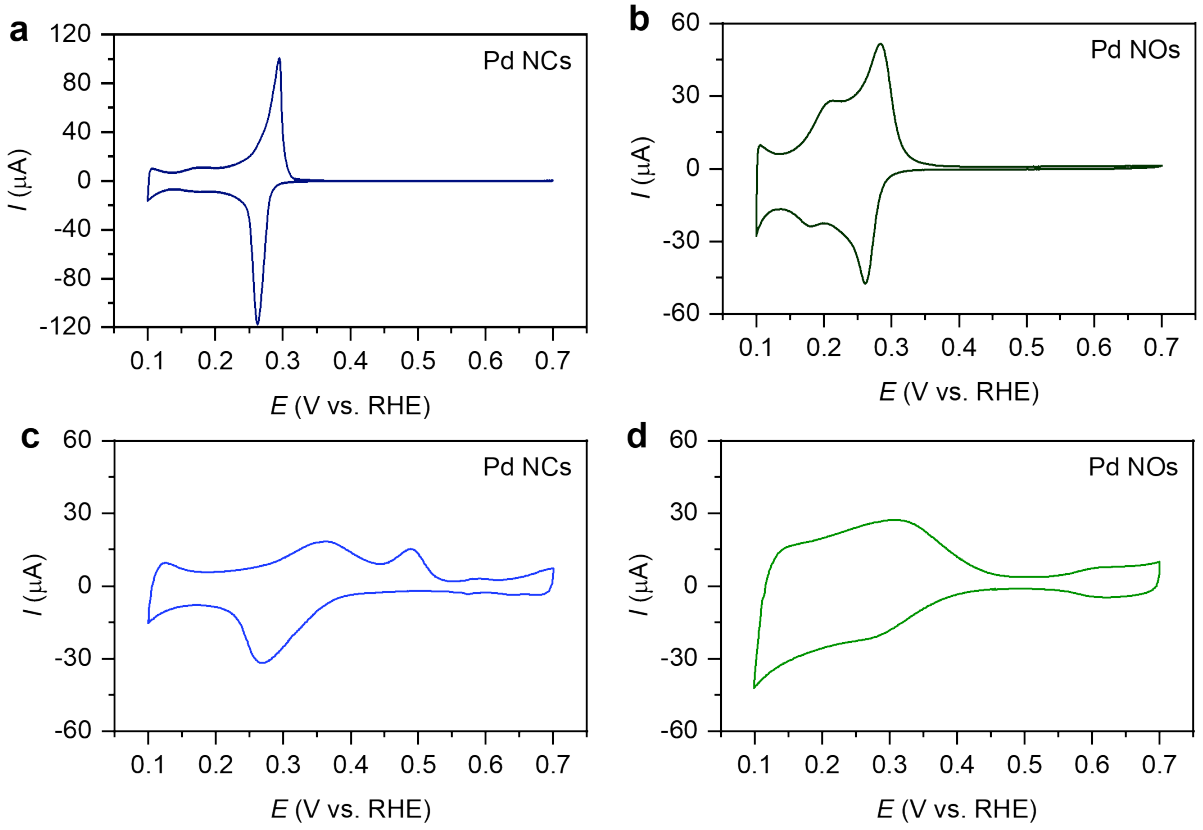

Figure 2. Cyclic voltammetry profiles for the Pd nanocubes (Pd NCs) and Pd nanooctahedrons (Pd NOs) recorded at $s = 5.00$ mV s^{-1} and T = 293 K in the 0.10–0.70 V potential range acquired in 0.50 M aqueous H_2SO_4 solution (the graphs **a** and **b**) and 0.10 M aqueous NaOH solution (the graphs **c** and **d**). They cover mainly the region of the under-potential deposition of H (UPD H).

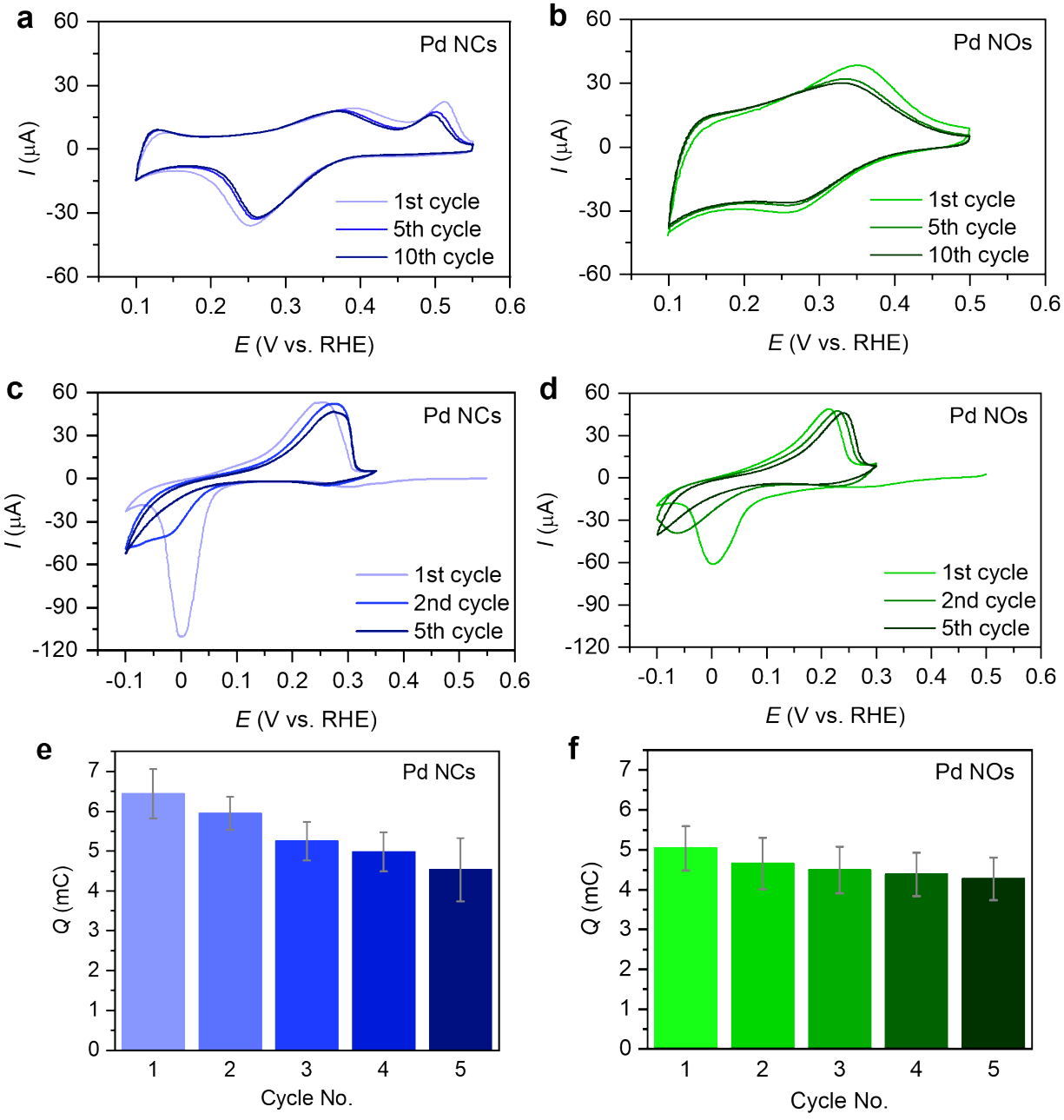

Figure 3. Cyclic voltammetry profiles (1st, 5th, and 10th) for the Pd nanocubes (Pd NCs) and Pd nanooctahedrons (Pd NOs) acquired in 0.10 M aqueous NaOH solution at $T = 293$ K. The graphs **a** and **b** cover the potential region of the UPD H (0.10 – 0.50 V) and the profiles are acquired at $s = 5.00$ mV s^{-1}. The graphs **c** and **d** cover the potential range of H absorption and

H_{abs} desorption and the profiles are acquired at $s = 1.0$ mV s^{-1}. The graphs **e** and **f** present the evolution of the charge (Q) for the desorption of H_{abs} as a function of the number of the potential transient for the Pd NCs (the graph **e**) and Pd NOs (the graph **f**). Each error bar represents the standard deviation of each charge value for three measurements, each employing a freshly prepared working electrode.

For comparative analysis, Figure 4 presents CV profiles for the Pd NCs and Pd NOs prior to and after the potential cycling in the region of the electrochemical H absorption and H_{abs} desorption by analyzing changes in the CV profiles associated with the UPD H and the onset of surface oxide formation, thus between $E = 0.10$ and $E = 0.70$ V. In the case of the Pd NCs, the cathodic peak initially at $E = 0.26$ V shifts to $E = 0.24$ V and its current slightly decreases. The current of the first anodic peak at $E = 0.35$ V also decreases but its potential remains the same; the second anodic peak shifts from $E = 0.49$ V to $E = 0.50$ V and its current slightly decreases. The value of the charge associated with the UPD H decreases from $Q = 912 \pm 25$ μC to $Q = 793 \pm 63$ μC (thus ca. 13%) after the potential cycling. The small CV features at the most-positive end of the CV profiles (between $E = 0.55$ V and $E = 0.70$ V) are due to the formation (anodic) and reduction (cathodic) of a surface oxide on the Pd NCs. The change in the associated charge is very small, from $Q = 101 \pm 7$ μC prior to and $Q = 99 \pm 7$ μC after the potential cycling. The difference between these

two values is so small that they are practically the same within the experimental uncertainty of the measurements. Thus, it may be concluded that the amount of the Pd surface oxide that is formed and reduced remains unaffected by the potential cycling. In the case of the Pd NOs, changes in the CV profiles prior to and after the potential cycling are more pronounced than in the case of the Pd NCs. A small cathodic peak (it is superimposed on a voltametric wave) initially observed at E = 0.30 V becomes a well-defined, large peak at E = 0.24 V; as the voltametric wave significantly alters its shape upon potential cycling, the peak's current increases. The well-defined anodic peak observed at E = 0.31 V shifts to a higher potential of E = 0.38 V, but its current remains practically the same. The value of the charge associated with the UPD H hardly changes, because it is Q = 1290 ± 60 μC prior to and 1300 ± 60 μC after the potential cycling. The initial anodic and cathodic features associated with the formation and reduction of a surface oxide on the Pd NOs are small (as in the case of the Pd NCs) and become well-defined after the potential cycling (unlike in the case of the Pd NCs). The change in the associated charge is significant because it increases from Q = 162 ± 12 μC to Q = 356 ± 24 μC (thus ca. 120%). Because the UPD H and surface oxide formation take place on the surface of the Pd NPs, the value of Q due to the UPD H or the surface oxide formation and reduction is a measure of the number of Pd surface atoms being in contact

with the electrolyte solution on which these processes can take place and the potential of the CV peaks is an indication of the surface arrangement of atoms. Thus, the change of Q is a measure of the number of Pd atoms added to or removed from the surface of the Pd NPs and the appearance or disappearance of peaks is an indication of surface structural changes.

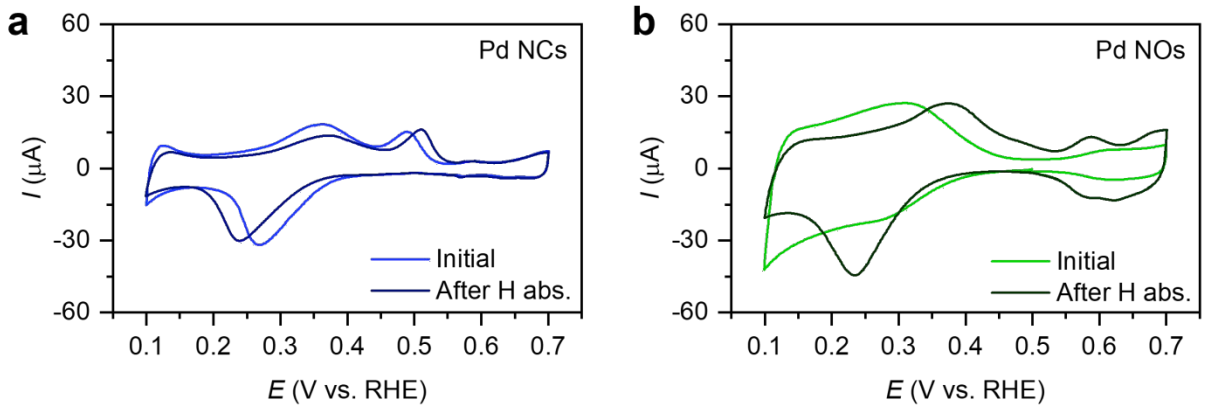

Figure 4. Cyclic voltammetry profiles for the Pd nanocubes (Pd NCs, the graph **a**) and Pd nanooctahedrons (Pd NOs, the graph **b**) recorded at $s = 5.00$ mV s^{-1} and $T = 293$ K in the 0.10–0.70 V potential range and acquired in 0.10 M aqueous NaOH solution. They cover mainly the region of the under-potential deposition of H (UPD H) and present CV profile acquired prior to and after five transients in the potential region of H absorption and H_{abs} desorption.

Carbon Monoxide Oxidative Desorption. Carbon monoxide (CO) stripping (oxidative desorption) is known to be a measure of the state of the surface of noble metal nanoparticles, because the shape of the respective CO stripping voltametric transient depends on the surface

arrangement of atoms. Figure 5 presents CO stripping voltametric transients for the Pd NCs and Pd NOs prior to (Figure 5a,c) and after (Figure 5b,d) potential cycling in the regions of electrochemical H absorption and H_{abs} desorption (the respective insets present the voltametric features associated with the UPD H, the onset of CO stripping, and the pre-peak). They also show CV profiles between $E = 0.10$ and $E = 1.00$ V right after the CO stripping (the gray transients), thus in the potential range of the UPD H and the surface oxide formation and reduction. In the case of the Pd NCs prior to the potential cycling in the region of H absorption and H_{abs} desorption, the CO stripping voltametric transient reveals an anodic pre-peak at $E = 0.39$ V and a well-defined asymmetric anodic peak at $E = 0.74$ V (Figure 5a). After potential cycling in the region of H absorption and H_{abs} desorption, the pre-peak remains mainly the same but the current of the main peak decreases and it develops a shoulder at $E = 0.76$ V (Figure 5b) and becomes broader. The presence of a pre-peak in the CO stripping voltametric transients was reported for Pt NPs in acidic and alkaline aqueous media.[34,35] The pre-peak for the CO stripping on the Pd NCs in 0.10 M aqueous NaOH solution appears at approximately the same potential as in the case of Pt NPs in alkaline media. Once CO has been stripped, the CV profiles for the Pd NCs show the usual features due to the UPD H in the potential range between $E = 0.10$ V and $E = 0.55$ V (they appear both

prior to and after potential cycling in the region of H absorption and H_{abs} desorption). In addition, the CV profiles reveal two anodic peaks at $E = 0.70$ V and $E = 0.87$ V and two cathodic peaks at $E = 0.76$ V and $E = 0.52$ V that are attributed to the formation and reduction of a surface oxide on the Pd NCs. The CO stripping transients allow us to determine the CO coverage (θ_{CO}), which is found to be $\theta_{CO} = 0.77$ prior to the potential cycling in the region of H absorption and H_{abs} desorption, and $\theta_{CO} = 0.81$ afterwards. In the case of the Pd NOs prior to the potential cycling in the region of H absorption and H_{abs} desorption, the CO stripping commences at $E = 0.50$ V and reveals well-defined anodic peaks at $E = 0.62$ V and $E = 0.76$ V, respectively (Figure 5c); an anodic pre-peak is not discernable. After potential cycling in the region of H absorption and H_{abs} desorption, the voltametric transient reveals a pre-peak (its current is low) at $E = 0.39$ V and a well-defined peak at $E = 0.76$ V; the peak's current is greater than prior to the potential cycling in the region of H absorption and H_{abs} desorption (Figure 5d). Following the CO stripping, the CV profile shows two anodic peaks at $E = 0.58$ V and $E = 0.69$ V and two cathodic ones at $E = 0.57$ V and $E = 0.72$ V characteristic of the formation of surface oxide and its reduction. As in the case of the Pd NCs, once CO is completely stripped (removed), the CV profile clearly shows the feature associated with the UPD H and the surface oxide formation and reduction. In other words, the

treatment of the Pd NCs and NOs that involves H absorption and H_{abs} desorption, and CO chemisorption and stripping does not affect their ability to electrochemically adsorb H (UPD) and to form a surface oxide. Again, the CO stripping transients allow us to determine the value of θ_{CO}, which is found to be $\theta_{CO} = 0.82$ prior to the potential cycling in the region of H absorption and H_{abs} desorption, and $\theta_{CO} = 0.78$ afterwards. In both cases of the Pd NCs and Pd NOs, the changes in the CO surface coverage are attributed to modification of the three-dimensional structure of the Pd NPs that bring about a change to the number of Pd surface atoms at which the CO chemisorption can take place.

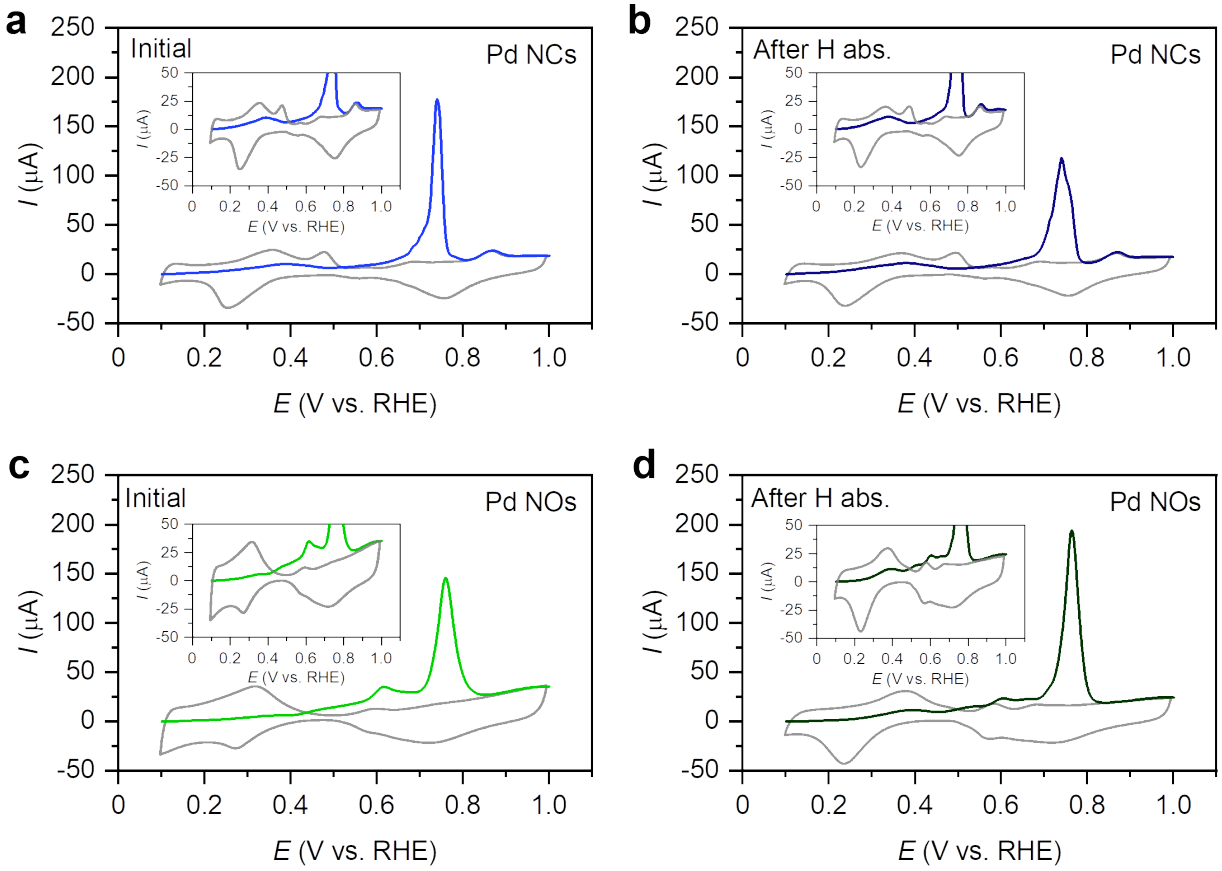

Figure 5. CO stripping voltametric transients for the Pd nanocubes (Pd NCs; the upper graphs) and Pd nanooctahedrons (Pd NOs; the lower graphs) recorded at $s = 5.00$ mV s^{-1} and $T = 293$ K in the 0.10–1.00 V potential range and acquired in 0.10 M aqueous NaOH solution. The transients were acquired prior to (the graphs **a** and **c**) and after (the graphs **b** and **d**) cycling in the potential region of H absorption and H_{abs} desorption.

In the case of Pd NPs, the electrochemical oxidation of chemisorbed CO (CO stripping) is expected to follow the Langmuir-Hinshelwood (L-H) mechanism or initially the Eley-Rideal (E-R) mechanism followed by the L-H one.[34] Which mechanism is operational depends on the vakue

of θ_{CO} and the presence of adsorbed oxygen-containing species on the surface of the nanomaterials. In the case of Pt NPs and a compressed CO overlayer having θ_{CO} = 0.83 and the process taking place in H_2SO_4 aqueous solutions, the E-R mechanism was found to be operational in the initial stage of the CO oxidative desorption at lower potentials followed by the L-H mechanism at higher potentials.[34] The E-R mechanism gives rise to the pre-peak, while the L-H mechanism to the main peaks. In alkaline media, the L-H mechanism is operational due to the presence of adsorbed OH,[36] although the initial stage of the reaction could still proceed according to the E-R mechanism if the CO overlayer is compressed. In the case of the Pd NPs, the voltametric features associated with the CO oxidative desorption are similar to those observed for the shape-controlled Pt NPs in alkaline media. In both cases, we observe a small pre-peak and two main peaks that are assigned to the process taking place on different terraces and kinks/steps.[35] Interestingly, in the case of shape-controlled Pt NPs and alkaline aqueous media, the shape of the voltametric features was found to be independent of the geometry of surface facets, unlike in the case of acidic aqueous media.[37] The results presented in Figure 5 clearly reveal that the shape of the CO stripping transients in aqueous alkaline media depends on the shape of the Pd NPs, thus is an indication of the surface arrangement of atoms.

The respective main facets of nanocubes and nanooctahedrons of fcc metals have the (100) and (111) surface structure, while their edges contain the (110) structure (the structure of corners is more complex). In the case of the Pd NCs, the pre-peak at $E = 0.39$ V is attributed to the (100) surface domains (facets) (Figure 5a,b). In the case of the Pd NOs, the CV features between $E = 0.50$ and $E = 0.70$ V are assigned to the (111) and (110) surface domains (facets) (Figure 5c,d). In the case of the Pd NCs prior to the cycling in the potential region of H absorption and H_{abs} desorption, the small shoulder at $E = 0.72$ V in the CV profile is assigned to the (110) surface domains (facets) (Figure 5a). In the case of the Pd NCs, the main CV peak associated with the CO oxidative desorption (striping) is observed at a lower potential than in the case of the Pd NOs, thus indicating that the process takes place more readily on the (100) surface domains as compared to the (111) ones (Figure 5a,c). The appearance of the pre-peak at $E = 0.40$ V observed for the Pd NOs after the potential cycling in the region of H absorption and H_{abs} desorption suggests that the treatment gives rise to the formation of a small fraction of (100) domains; thus, the shape of the Pd NOs is changed. In the case of the Pd NCs after potential cycling in the region of H absorption and H_{abs} desorption, the current of the main CV peak associated with the CO oxidative desorption decreases and a shoulder at $E = 0.76$ V develops. This shoulder appears at the same potential as

the CO oxidative desorption peak in the case of the Pd NOs, thus suggesting that the shape of the Pd NC undergoes a slight change and that (111) surface domains develop due to the potential cycling in the region of H absorption and H_{abs} desorption.

Identical Location-Transmission Electron Microscopy (IL-TEM) Analysis. The outcome of the electrochemical measurements clearly reveals that H absorption and H_{abs} desorption bring about irreversible structural changes in the shape-controlled Pd NPs in alkaline aqueous medium. It is important to highlight that our previous study did not reveal any structural changes when the Pd NPs underwent the same treatment (H absorption and H_{abs} desorption) in acidic aqueous medium, and identical location-transmission electron microscopy (IL-TEM) images showed that their shape was preserved.[29] The remarkable stability of the shape-controlled Pd NPs was attributed to the lack of structural defects and grain boundaries that are ubiquitous in the case of polycrystalline Pd materials. It needs to be emphasized that these structural imperfections, especially grain boundaries, give rise to pulverization of polycrystalline Pd and other H-absorbing materials upon repetitive H absorption and H_{abs} desorption. In the present study, the size of the Pd NCs and Pd NOs is determined to be in the 7–13 nm (Pd NCs) and 4–9 nm (Pd NOs) ranges giving an average particle size of 9.8 nm and 6.9 nm (Figure 6a,d), respectively. It is important to mention that the

size of the Pd NCs and Pd NOs employed in this research is practically the same as in the case of the Pd NPs used in the previous work (acidic aqueous media).[23,29] The Pd NPs employed in this research were also examined by acquiring CV profiles in acidic aqueous media and the results were found to be in excellent agreement with our previous results. Thus, it may be concluded that within the experimental uncertainty, the Pd NPs employed in the current and past research projects are practically the same, thus possess the same shape and size.

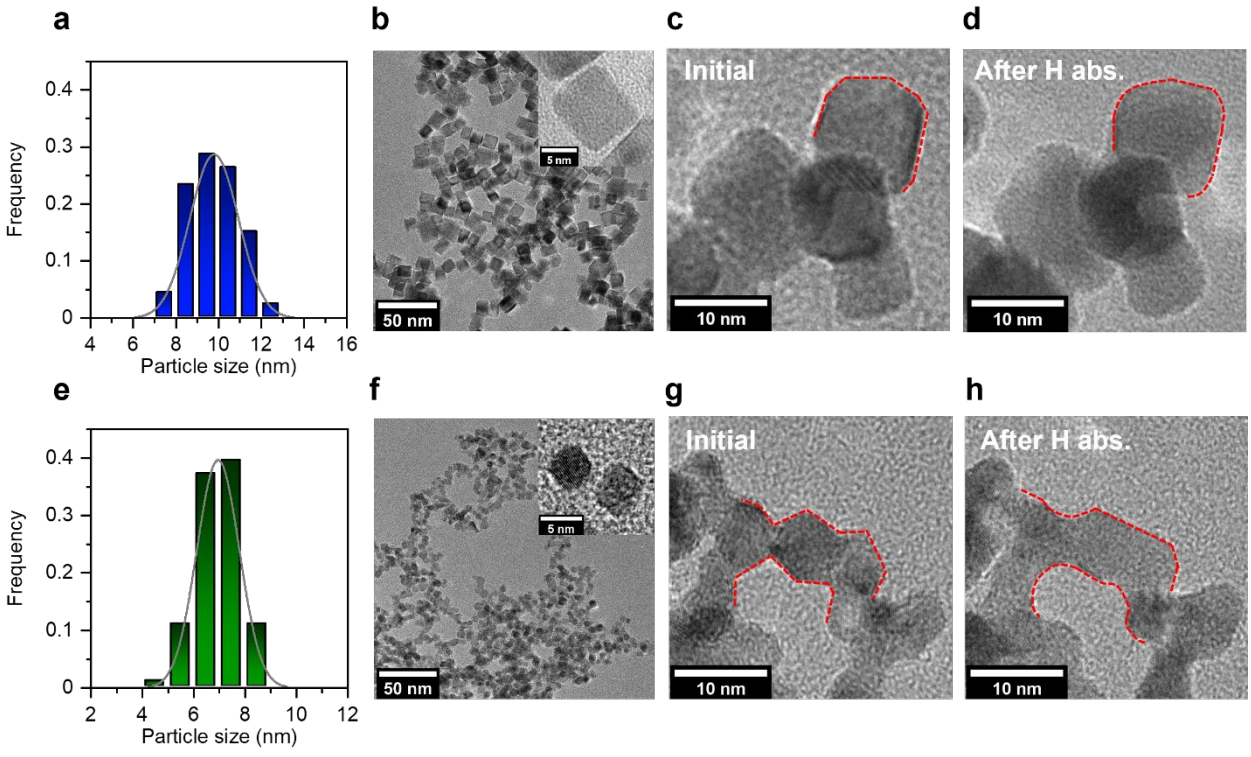

Figure 6. Size distributions (the graphs **a** and **e**) and TEM images (the graphs **b** and **f**) of freshly-prepared Pd NPs. IL-TEM images prior to (the graphs **c** and **g**) and after (the graphs **d** and **h**) potential cycling in the potential region of H absorption and H_{abs} desorption. The upper

graphs refer to the Pd nanocubes (Pd NCs) and the lower graphs to the Pd nanooctahedrons (Pd NOs).

An IL-TEM analysis was conducted to verify the shape of the Pd NPs after their preparation and to examine any changes in their shape after repetitive H absorption and H_{abs} desorption. The IL-TEM images revealed that the Pd NCs had an initial cubic shape and that their edges became rounded after the potential cycling (Figure 6b-d) and the Pd NOs had an initial octahedral shape and that their edges also became rounded after the potential cycling (Figure 6e-g). The loss of edges by the Pd NCs and Pd NOs not only alters their shape but also modifies the fraction of the initially oriented surfaces, the (100) facets in the case of the Pd NCs and the (111) facets in the case of the Pd NOs. These structural changes give rise to different CV profiles than those acquired prior to their electrochemical treatment involving H absorption and H_{abs} desorption. Figure 3e,f indicated that the amount of desorbed H_{abs} decreases as the number of H absorption and H_{abs} desorption cycles increases. We attribute the decrease in the amount of desorbed H_{abs} and the structural changes to H trapping inside of the Pd NCs and Pd NOs. Such a behavior was also observed for Pd NPs with average sizes of less than 6 nm upon H absorption and H_{abs} desorption in the gas phase.[38–40] A computational study indicated that the trapped H was stabilized in

subsurface octahedral sites and that the trapped H atoms formed a strong bond with Pd host atoms. The trapping of H atoms brings about structural stress that is released by modifying the shape of the Pd NPs.[41] In fact, it was observed that the trapped H even requires an elevated temperature and considerable vacuum condition to be completely desorbed from the Pd NPs. Thus, the increased temperature and higher vacuum (lowered pressure) corroborate the computation study indicating that the trapped H formed a strong bond with the host Pd atoms.

Based upon existing literature data and our experimental results, we propose that in the case of H absorption and H_{abs} desorption under electrochemical conditions, the process induces H trapping and structural changes, but this behavior is only observed in alkaline aqueous medium, as no structural changes or H trapping were observed in acidic aqueous medium. The mechanism of the H diffusion inside the Pd NPs does not depend on the composition of the aqueous electrolyte solution because the H_{abs} species being inside the bulk of the metal host does not experience the interface (it does not directly interact with it). However, the source of the electrochemically adsorbed H (H_{UPD}) and of the electrochemically absorbed H (H_{abs}) is different in alkaline and acidic aqueous media. In both cases, an electron transfer and an ion transfer take place, and H_3O^+ is the source of H_{abs} and H_2O is the product of the process in acidic aqueous media ($H_3O^+ + e^- \rightarrow H_{abs} +$

H_2O), and H_2O is the source of H_{abs} and OH^- is the product of the process in alkaline aqueous media ($H_2O + e^- \rightarrow H_{abs} + OH^-$). Since the electron transfer is faster than the ion transfer, the processes of the electrochemical H adsorption and H absorption is expected to be influenced by the ion transfer (H_3O^+ and OH^- in acidic and alkaline aqueous media, respectively) through the Pd electrode/aqueous electrolyte solution interface. A recent study of the kinetics of the UPD H on monocrystalline Pt electrodes indicated that the ion transfer in alkaline aqueous media (the OH^- transfer) is slower in alkaline media than that in acidic ones due to the formation of a rigid water network adjacent to the electrode surface.[42,43] As an alternative proposal, it was reported that hydrated cations interact with adsorbed OH on monocrystalline Pt electrodes and influence the kinetics of fuel cell reactions by forming a "quasi-specifically" adsorbed state on the Pt surface.[44] In the light of this knowledge and bearing in mind many similarities in the electrochemical behavior of Pt and Pd materials, we propose that the water network adjacent to the surface of the Pd NPs or the interaction between hydrated cations and adsorbed OH has a significant impact on the desorption of H_{abs} resulting in some of it being trapped along edges of the Pd NPs.

Comparative Analysis of the H Absorption and H_{abs} Desorption in Acidic and Alkaline Aqueous Media. Figure 7 shows CV profiles for freshly prepared Pd NCs and Pd NOs in the potential range

of the UPD H, H absorption and H_{abs} desorption obtained in 0.50 M aqueous H_2SO_4, 0.10 M aqueous $HClO_4$, and 0.10 M aqueous NaOH solutions and acquired at $s = 1.00$ mV s^{-1} and $T = 293$ K. The graphs in the first row refer to the Pd NCs and those in the second row refer to the Pd NOs. The cathodic and anodic peak potentials ($E_{p,cath}$ and $E_{p,an}$) and the respective differences between the anodic and cathodic peak potentials ($\Delta E_p = E_{p,an} - E_{p,cath}$) are summarized in Table 1. In the case of the acidic media (H_2SO_4 and $HClO_4$), the CV peaks due to H absorption and H_{abs} desorption are sharp and narrow. In the case of the 0.10 M aqueous NaOH solution, the CV peaks due to H absorption and H_{abs} desorption are less sharp and broader. The features associated with the UPD H are very small because the CV transients are recorded at $s = 1.00$ mV s^{-1} and the process gives rise to a very small pseudo-capacitive current (the pseudocapacitive current is linearly proportional to the potential scan rate and is very small for $s = 1.00$ mV s^{-1}). On the other hand, the low potential scan rate favors H absorption in the sense that the Pd NPs experience a potential at which the process can take place for a longer time, thus more H becomes absorbed as the value of s decreases. While the H absorption and H_{abs} desorption behavior of the Pd NCs and Pd NOs is very similar in the aqueous H_2SO_4 and $HClO_4$ solutions, it is qualitatively different in the 0.10 M aqueous NaOH one. Specifically, in addition to the cathodic and anodic peaks being less sharp and broader in the

0.10 M aqueous NaOH solution, the anodic peak appears at a significantly higher potential than in the case of the H_2SO_4 and $HClO_4$ solutions (Table 1). This observation suggests that the sub-surface H (H_{ss}; see Figure 1) is bonded stronger in the alkaline medium than in the acidic ones and this behavior is attributed to the water network formed and being adjacent to the surface of the Pd NPs or the interaction of hydrated cations with the adsorbed OH on the NP surface in the aqueous alkaline medium, which possibly impacts the last step of H desorption. It is important to add that the cathodic peak associated with H absorption is observed at the same potential in the three aqueous electrolyte solutions, while the anodic peak in the case of the 0.10 M aqueous NaOH solution appears at a much higher potential (*ca.* at 0.165 V and 0.120 V higher in the case of the Pd NCs and Pd NOs, respectively).

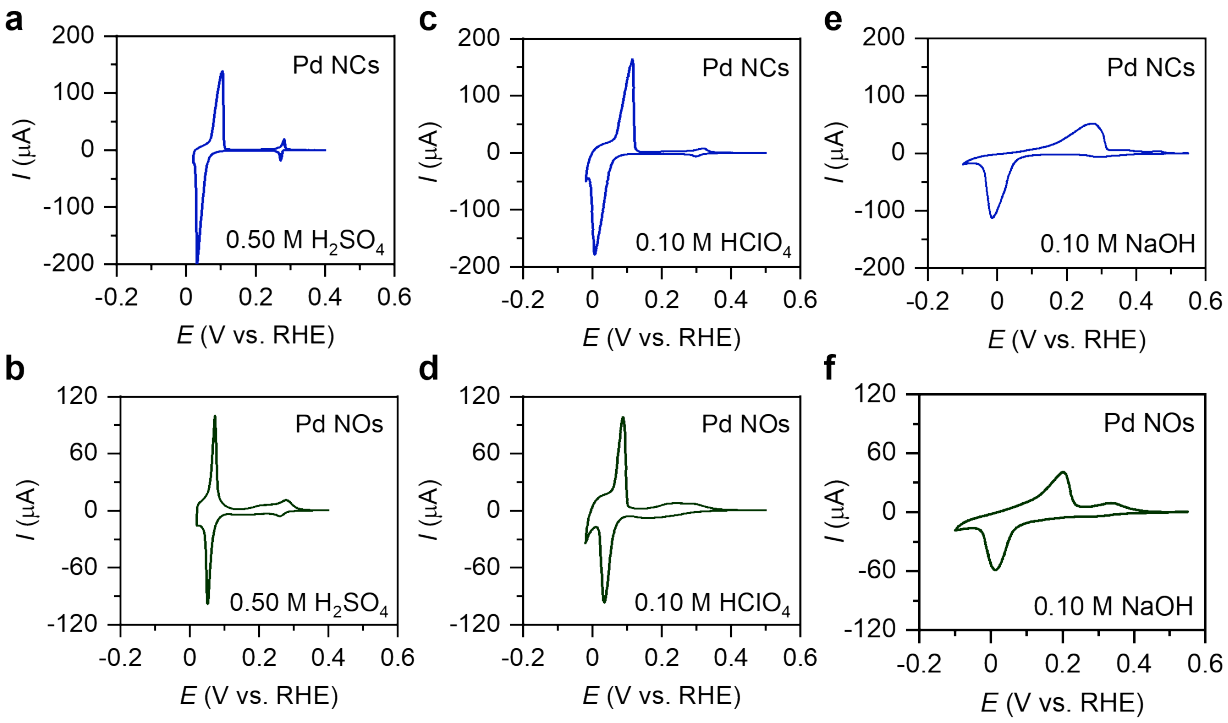

Figure 7. CV profiles for freshly prepared Pd nanocubes (Pd NCs, the graphs **a**, **c**, and **e**) and Pd nanooctahedrons (Pd NOs, the graphs **b**, **d**, and **f**) in the potential range of the UPD H, H absorption, and H_{abs} desorption obtained in 0.50 M aqueous H_2SO_4, 0.10 M aqueous $HClO_4$, and 0.10 M aqueous NaOH solutions and acquired at $s = 1.00$ mV s^{-1} and $T = 293$ K.

Table 1. Values of the cathodic and anodic peak potentials ($E_{p,cath}$ and $E_{p,an}$) and their difference ΔE_p ($\Delta E_p = E_{p,an} - E_{p,cath}$)

	$E_{p,cath}$	$E_{p,an}$	ΔE_p
Pd nanocubes			
0.50 M H_2SO_4	0.031 V	0.103 V	0.072 V
0.10 M $HClO_4$	0.007 V	0.110 V	0.103 V
0.10 M NaOH	−0.014 V	0.276 V	0.290 V
Pd nanooctahedrons			
0.50 M H_2SO_4	0.049 V	0.085 V	0.036 V
0.10 M $HClO_4$	0.034 V	0.087 V	0.053 V
0.10 M NaOH	0.012 V	0.207 V	0.195 V

Figure 3 presented the evolution (decrease) of the Q values upon repetitive cycling of Pd NCs and Pd NOs in the potential range of H absorption and H_{abs} desorption in the 0.10 M aqueous NaOH solution, which pointed to H trapping in the Pd NCs and Pd NOs. Bearing in mind the results shown in Figure 7, we relate this behavior to the structure of water molecules adjacent to the NP surface or the interaction between hydrated cations and adsorbed OH on the Pd NPs surface. To further examine this behavior, we integrated the CV profiles presented in Figure 7 and determined the total charge associated with H absorption and H_{abs} desorption in the three aqueous

media (Figure 8). In the case of the aqueous H_2SO_4 and $HClO_4$ solutions, the cathodic (H absorption) and anodic (H_{abs} desorption) charge values agree within the experimental uncertainty, but in the case of the aqueous NaOH solution the cathodic charge value is significantly higher than the anodic one (15% for the Pd NCs and 19% for the Pd NOs). The unbalanced charge values are a measure of the amount of trapped H in the Pd NPs. As mentioned above, in the case of gas-phase experiments, H trapped in Pd NPs requires higher desorption temperatures and higher vacuum (lower pressure) and, consequently, under electrochemical conditions this would translate into the application of higher potentials.[40,41] The quantification of the amount of H trapped in the Pd NCs and Pd NOs is not straightforward, because we would have to apply higher potentials than 0.55 V (0.55 V is the upper potential limit of the CV profiles shown in Figure 7). Since the formation of the Pd surface oxide commences at *ca.* 0.60 V, it would be practically impossible to deconvolute such CV transients to determine the charges due to the surface oxide formation and the desorption of trapped H. Consequently, a comparison of the cathodic and anodic charges is the only viable approach to assess the amount of the incompletely desorbed (trapped) H. It is interesting to observe that in the case of H trapping in Pd NPs under gas-phase conditions, the amount of trapped H is *ca.* 26% of the initial H capacity.[41] This value is in good agreement with

the above reported values, 15% for the Pd NCs and 19% for the Pd NOs, although the experimental conditions are very different.

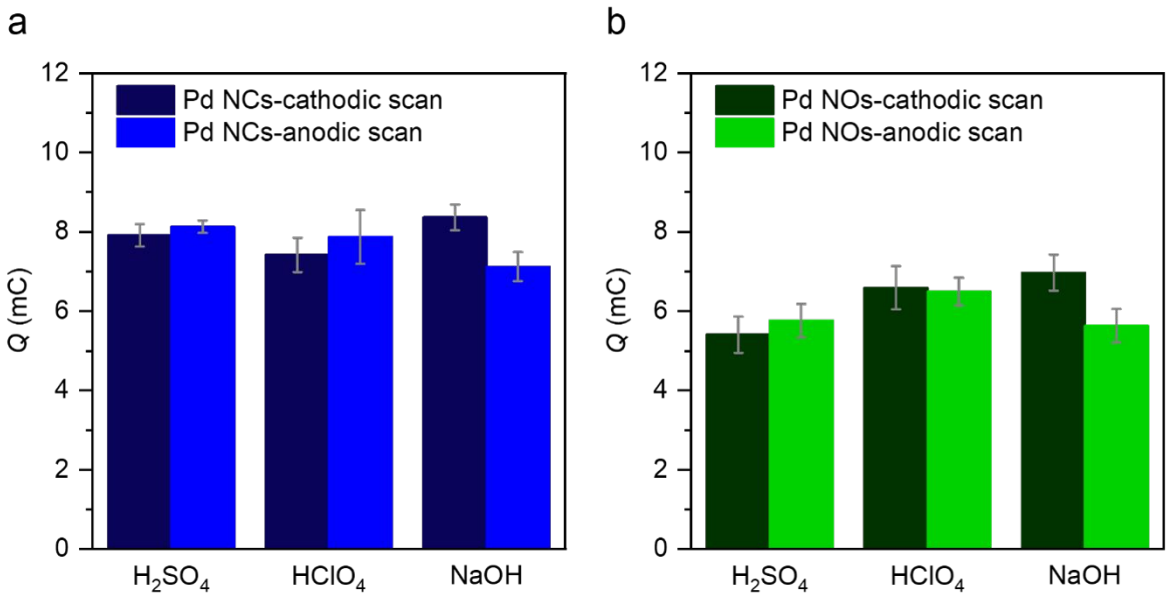

Figure 8. Charge (Q) values for the Pd nanocubes (Pd NCs, the graph **a**) and Pd nanooctahedrons (Pd NOs, the graph **b**) determined by integrating the cathodic and anodic components of the CV profiles presented in Figure 7. Each error bar represents the standard deviation of each charge value for three separate measurements, each employing a freshly prepared working electrode.

CONCLUSIONS

The electrochemical behavior of Pd NCs and Pd NOs in alkaline aqueous medium was investigated in the potential region of H absorption and H_{abs} desorption (the UPD H also occurs

but its charge is very small compared to the charge of H absorption and H_{abs} desorption). The Pd NCs and Pd NOs remained stable in the potential region of the UPD H, while repetitive potential cycling in the region of H absorption and H_{abs} desorption induced irreversible structural changes. The existence of modification of the surface structure of the Pd NPs was deduced by analyzing changes in the charge associated with the UPD H after the repetitive potential cycling. The shape of the CO stripping transients also underwent modification, as a result of the repetitive potential cycling indicating that the fraction of oriented facets in the Pd NCs and Pd NOs was also modified. These observations were supported by the results of identical location-transmission electron microscopy (IL-TEM) analyses, which revealed that the Pd NCs and Pd NOs lost their edges and corners, again after the repetitive potential cycling in the region of H absorption and H_{abs} desorption. We also observed that the amount of H_{abs} decreased upon the potential cycling and the associated structural changes of the Pd NPs were attributed to H trapping in the near-surface region of the Pd NPs. Hydrogen trapping creates structural strain that leads to the shape modification of the Pd NPs. This behavior of the Pd NCs and Pd NOs was uniquely observed in alkaline aqueous medium, as no structural changes or H trapping were observed in acidic aqueous medium. On the basis of our electrochemical and materials science experiments and bearing in

mind the existing knowledge, we proposed that the structure of water network adjacent to the surface of the Pd NPs or the interaction between hydrated cations and adsorbed OH on the NP surface impacts (hinders) the energetics of H_{abs} desorption in alkaline aqueous medium. We also performed a comparative analysis of the behavior of the Pd NPs by conducting experiments in acidic and alkaline aqueous media (H_2SO_4, $HClO_4$, and NaOH aqueous solutions), which revealed that the CV feature (peak) due to H absorption was at the same potential but the CV feature (peak) due to H_{abs} desorption was at a significantly higher potential in alkaline aqueous medium. A comparison of the cathodic (absorption) and anodic (desorption) charge values pointed to some H_{abs} remaining inside of the Pd NPs (being trapped). These results support the initial proposal that the network of water molecules or the interaction between hydrated cations and adsorbed OH hinders H desorption and results in some of it being trapped. This study is a continuation of previous research on H absorption in Pd NPs and provided new knowledge and reports on a unique behavior of shape-controlled Pd NPs in aqueous alkaline medium in the potential range of electrochemical H absorption and H_{abs} desorption. Since Pd is known to be an excellent H host and serves as a model hydrogen-absorbing material, we hope that the outcome of this study will benefit electrochemical nanomaterials science and the field of energy storage materials.

AUTHOR INFORMATION

Corresponding Authors

Christophe Coutanceau – IC2MP, UMR CNRS 7285, Université de Poitiers, 4 rue Michel Brunet, TSA 51106, 86073, Poitiers Cedex 9, France; Phone: (5) 49 36 64 14; Email: christophe.coutanceau@univ-poitiers.fr

Gregory Jerkiewicz – Department of Chemistry, Queen's University, Kingston, Ontario K7L 3N6, Canada; Phone: (613) 533-6413; Email: gregory.jerkiewicz@queensu.ca

Author Contributions

The manuscript was written through contributions of all authors. All authors have given approval to the final version of the manuscript.

Notes

The authors declare no competing financial interest.

ACKNOWLEDGMENT

This research was conducted as part of the Engineered Nickel Catalysts for Electrochemical Clean Energy project administered from Queen's University and supported by Grant NO. RGPNM 477963-2015 under the Natural Sciences and Engineering Research Council of Canada (NSERC) Discovery Frontiers Program. S.F. gratefully acknowledges financial support for international travel from the Mitacs Globalink Research Award and The Sabin Metal Ron Bleggi Student Award from the International Precious Metals Institute. S.B. and C.C. acknowledge support toward their international travel from the "Ni Electro Can" project. We thank Dr. Kevin McEleney at Queen's University for conducting TEM analysis.

REFERENCES

(1) Graham, T. XVIII. On the Absorption and Dialytic Separation of Gases by Colloid Septa. *Philos. Trans. R. Soc.* **1866**, *156*, 339–439.

(2) Li, G.; Kobayashi, H.; Dekura, S.; Ikeda, R.; Kubota, Y.; Kato, K.; Takata, M.; Yamamoto, T.; Matsumura, S.; Kitagawa, H. Shape-Dependent Hydrogen-Storage Properties in Pd Nanocrystals: Which Does Hydrogen Prefer, Octahedron (111) or Cube (100)? *J. Am. Chem. Soc.* **2014**, *136* (29), 10222–10225.

(3) Ramos-Castillo, C. M.; Reveles, J. U.; Zope, R. R.; De Coss, R. Palladium Clusters Supported on Graphene Monovacancies for Hydrogen Storage. *J. Phys. Chem. C* **2015**, *119* (15), 8402–8409.

(4) Yamauchi, M.; Ikeda, R.; Kitagawa, H.; Takata, M. Nanosize Effects on Hydrogen Storage in Palladium. *J. Phys. Chem. C* **2008**, *112* (9), 3294–3299.

(5) Lange, U.; Hirsch, T.; Mirsky, V. M.; Wolfbeis, O. S. Hydrogen Sensor Based on a Graphene-Palladium Nanocomposite. *Electrochim. Acta* **2011**, *56* (10), 3707–3712.

(6) Chiu, C. Y.; Huang, M. H. Polyhedral Au-Pd Core-Shell Nanocrystals as Highly Spectrally Responsive and Reusable Hydrogen Sensors in Aqueous Solution. *Angew. Chemie - Int. Ed.* **2013**, *52* (48), 12709–12713.

(7) Tang, J.; Yamamoto, S.; Koitaya, T.; Yoshikura, Y.; Mukai, K.; Yoshimoto, S.; Matsuda, I.; Yoshinobu, J. Hydrogen Adsorption and Absorption on a Pd-Ag Alloy Surface Studied Using in-Situ X-Ray Photoelectron Spectroscopy under Ultrahigh Vacuum and Ambient Pressure. *Appl. Surf. Sci.* **2019**, *463*, 1161–1167.

(8) Ye, X. R.; Lin, Y.; Wai, C. M. Decorating Catalytic Palladium Nanoparticles on Carbon

Nanotubes in Supercritical Carbon Dioxide. *Chem. Commun.* **2003**, *3* (5), 642–643.

(9) Bai, X.; Chen, W.; Zhao, C.; Li, S.; Song, Y.; Ge, R.; Wei, W.; Sun, Y. Exclusive Formation of Formic Acid from CO_2 Electroreduction by a Tunable Pd-Sn Alloy. *Angew. Chemie Int. Ed.* **2017**, *56* (40), 12219–12223.

(10) Green, S. K.; Lee, J.; Kim, H. J.; Tompsett, G. A.; Kim, W. B.; Huber, G. W. The Electrocatalytic Hydrogenation of Furanic Compounds in a Continuous Electrocatalytic Membrane Reactor. *Green Chem.* **2013**, *15* (7), 1869–1879.

(11) Song, Y.; Sanyal, U.; Pangotra, D.; Holladay, J. D.; Camaioni, D. M.; Gutiérrez, O. Y.; Lercher, J. A. Hydrogenation of Benzaldehyde via Electrocatalysis and Thermal Catalysis on Carbon-Supported Metals. *J. Catal.* **2018**, *359*, 68–75.

(12) Jerkiewicz, G. Hydrogen Sorption at/in Electrodes. *Prog. Surf. Sci.* **1998**, *57* (2), 137–186.

(13) Qian, S. Y.; Conway, B. E.; Jerkiewicz, G. Comparative Effects of Adsorbed S-Species on H Sorption into Pd from UPD and OPD; A Kinetic Analysis. *Int. J. Hydrogen Energy* **2000**, *25* (3), 539–550.

(14) Jerkiewicz, G. Electrochemical Hydrogen Adsorption and Absorption. Part 1: Under-

Potential Deposition of Hydrogen. *Electrocatalysis* **2010**, *1* (4), 179–199.

(15) Baldauf, M.; Kolb, D. M. A Hydrogen Adsorption and Absorption Study with Ultrathin Pd Overlayers on Au(111) and Au(100). *Electrochim. Acta* **1993**, *38* (15), 2145–2153.

(16) Czerwinski, A.; Marassi, R. The Absorption of Hydrogen and Deuterium in Thin Palladium Electrodes Part II: Basic Solutions. *J. Electroanal. Chem* **1992**, *322*, 373–381.

(17) Duncan, H.; Lasia, A. Mechanism of Hydrogen Adsorption/Absorption at Thin Pd Layers on Au(111). *Electrochim. Acta* **2007**, *52* (21), 6195–6205.

(18) Martin, M. H.; Lasia, A. Hydrogen Sorption in Pd Monolayers in Alkaline Solution. *Electrochim. Acta* **2009**, *54* (22), 5292–5299.

(19) Sherbo, R. S.; Moreno-Gonzalez, M.; Johnson, N. J. J.; Dvorak, D. J.; Fork, D. K.; Berlinguette, C. P. Accurate Coulometric Quantification of Hydrogen Absorption in Palladium Nanoparticles and Thin Films. *Chem. Mater.* **2018**, *30* (12), 3963–3970.

(20) Rose, A.; Maniguet, S.; Mathew, R. J.; Slater, C.; Yao, J.; Russell, A. E. Hydride Phase Formation in Carbon Supported Palladium Nanoparticle Electrodes Investigated Using in Situ EXAFS and XRD. *Phys. Chem. Chem. Phys.* **2003**, *5* (15), 3220–3225.

(21) Tateishi, N.; Yahikozawa, K.; Nishimura, K.; Takasu, Y. Hydrogen Electrode Reaction on Electrodes of Glassy Carbon-Supported Ultrafine Pd Particles in Alkaline Media. *Electrochim. Acta* **1992**, *37* (13), 2427–2432.

(22) Tateishi, N.; Yahikozawa, K.; Nishimura, K.; Suzuki, M.; Iwanaga, Y.; Watanabe, M.; Enami, E.; Matsuda, Y.; Takasu, Y. Electrochemical Properties of Ultra-Fine Palladium Particles for Adsorption and Absorption of Hydrogen in an Aqueous $HClO_4$ Solution. *Electrochim. Acta* **1991**, *36* (7), 1235–1240.

(23) Zalineeva, A.; Baranton, S.; Coutanceau, C.; Jerkiewicz, G. Electrochemical Behavior of Unsupported Shaped Palladium Nanoparticles. *Langmuir* **2015**, *31*, 1605–1609.

(24) Kibler, L. A.; El-Aziz, A. M.; Hoyer, R.; Kolb, D. M. Tuning Reaction Rates by Lateral Strain in a Palladium Monolayer. *Angew. Chemie - Int. Ed.* **2005**, *44* (14), 2080–2084.

(25) Hara, M.; Linke, U.; Wandlowski, T. Preparation and Electrochemical Characterization of Palladium Single Crystal Electrodes in 0.1 M H_2SO_4 and $HClO_4$. Part I. Low-Index Phases. *Electrochim. Acta* **2007**, *52* (18), 5733–5748.

(26) Grdén, M.; Łukaszewski, M.; Jerkiewicz, G.; Czerwínski, A. Electrochemical Behaviour of

Palladium Electrode: Oxidation, Electrodissolution and Ionic Adsorption. *Electrochim. Acta* **2008**, *53*, 7583–7598.

(27) Gabrielli, C.; Grand, P. P.; Lasia, A.; Perrot, H. Investigation of Hydrogen Adsorption and Absorption in Palladium Thin Films. *J. Electrochem. Soc.* **2004**, *151* (11), A1937–A1942.

(28) Duncan, H.; Lasia, A. Separation of Hydrogen Adsorption and Absorption on Pd Thin Films. *Electrochim. Acta* **2008**, *53* (23), 6845–6850.

(29) Zalineeva, A.; Baranton, S.; Coutanceau, C.; Jerkiewicz, G. Octahedral Palladium Nanoparticles as Excellent Hosts for Electrochemically Adsorbed and Absorbed Hydrogen. *Sci. Adv.* **2017**, *3* (2), e1600542.

(30) Li, D.; Wang, C.; Tripkovic, D.; Sun, S.; Markovic, N. M.; Stamenkovic, V. R. Surfactant Removal for Colloidal Nanoparticles from Solution Synthesis: The Effect on Catalytic Performance. *ACS Catal.* **2012**, *2* (7), 1358–1362.

(31) Rafaïdeen, T.; Baranton, S.; Coutanceau, C. Pd-Shaped Nanoparticles Modified by Gold Ad-Atoms: Effects on Surface Structure and Activity toward Glucose Electrooxidation. *Front. Chem.* **2019**, *7*, 453.

(32) Hoshi, N.; Nakamura, M.; Maki, N.; Yamaguchi, S.; Kitajima, A. Structural Effects on Voltammograms of the Low Index Planes of Palladium and Pd(S)-[*n*(100) × (111)] Surfaces in Alkaline Solution. *J. Electroanal. Chem.* **2008**, *624* (1–2), 134–138.

(33) Kiguchi, F.; Nakamura, M.; Hoshi, N. Structural Effects on Voltammograms of the High Index Planes of Pd in Alkaline Solution. *J. Electroanal. Chem.* **2021**, *880*, 114925.

(34) Urchaga, P.; Baranton, S.; Coutanceau, C.; Jerkiewicz, G. Evidence of an Eley-Rideal Mechanism in the Stripping of a Saturation Layer of Chemisorbed CO on Platinum Nanoparticles. *Langmuir* **2012**, *28* (36), 13094–13104.

(35) Farias, M. J. S.; Vidal-Iglesias, F. J.; Solla-Gullón, J.; Herrero, E.; Feliu, J. M. On the Behavior of CO Oxidation on Shape-Controlled Pt Nanoparticles in Alkaline Medium. *J. Electroanal. Chem.* **2014**, *716*, 16–22.

(36) Spendelow, J. S.; Goodpaster, J. D.; Kenis, P. J. A.; Wieckowski, A. Mechanism of CO Oxidation on Pt(111) in Alkaline Media. *J. Phys. Chem. B* **2006**, *110* (19), 9545–9555.

(37) Urchaga, P.; Baranton, S.; Coutanceau, C.; Jerkiewicz, G. Electro-Oxidation of CO Chem on Pt Nanosurfaces: Solution of the Peak Multiplicity Puzzle. *Langmuir* **2012**, *28* (7), 3658–

3663.

(38) Jose, D.; Jagirdar, B. R. Nature of Hydrogen Atom Trapped inside Palladium Lattice. *Int. J. Hydrogen Energy* **2010**, *35* (13), 6804–6811.

(39) Ren, H.; Zhang, T. Y. H Concentrations and Stresses in Pd Nanoparticles. *Mater. Lett.* **2014**, *130*, 176–179.

(40) Kobayashi, H.; Yamauchi, M.; Kitagawa, H.; Kubota, Y.; Kato, K.; Takata, M. On the Nature of Strong Hydrogen Atom Trapping inside Pd Nanoparticles. *J. Am. Chem. Soc.* **2008**, *130* (6), 1828–1829.

(41) Liu, W.; Magnin, Y.; Förster, D.; Bourgon, J.; Len, T.; Morfin, F.; Piccolo, L.; Amara, H.; Zlotea, C. Size-Dependent Hydrogen Trapping in Palladium Nanoparticles. *J. Mater. Chem. A* **2021**, *9* (16), 10354–10363.

(42) Rizo, R.; Sitta, E.; Herrero, E.; Climent, V.; Feliu, J. M. Towards the Understanding of the Interfacial pH Scale at Pt(111) Electrodes. *Electrochim. Acta* **2015**, *162*, 138–145.

(43) Ledezma-Yanez, I.; Wallace, D.; Sebastian-Pascual, P.; Climent, V.; Feliu, J. M.; Koper, M. T. M. Interfacial Water Reorganization as a pH-Dependent Descriptor of the Hydrogen

Evolution Rate on Platinum Electrodes. *Nat. Energy* **2017**, *2*, 17031.

(44) Strmcnik, D.; Kodama, K.; Van Der Vliet, D.; Greeley, J.; Stamenkovic, V. R.; Marković, N. M. The Role of Non-Covalent Interactions in Electrocatalytic Fuel-Cell Reactions on Platinum. *Nat. Chem.* **2009**, *1* (6), 466–472.

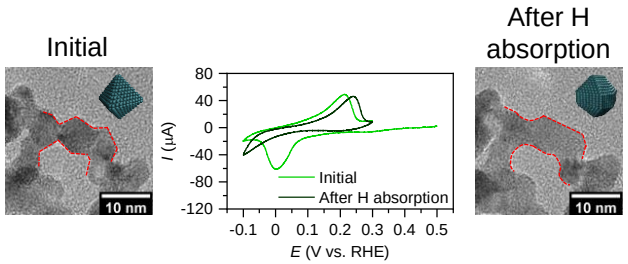

Graphical abstract

ACS Paragon Plus Environment

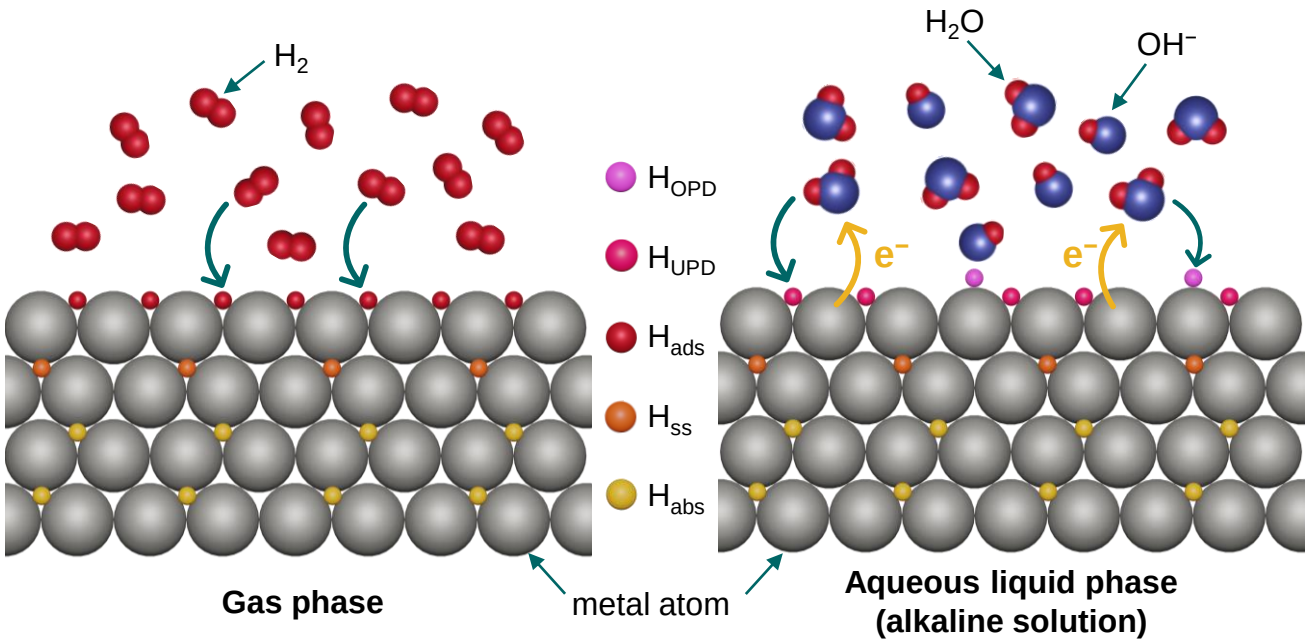
H2
H2O
OH−
HOPD
HUPD
Hads
Hss
Habs
e−
e−
Gas phase
metal atom
Aqueous liquid phase
(alkaline solution)

Figure 1

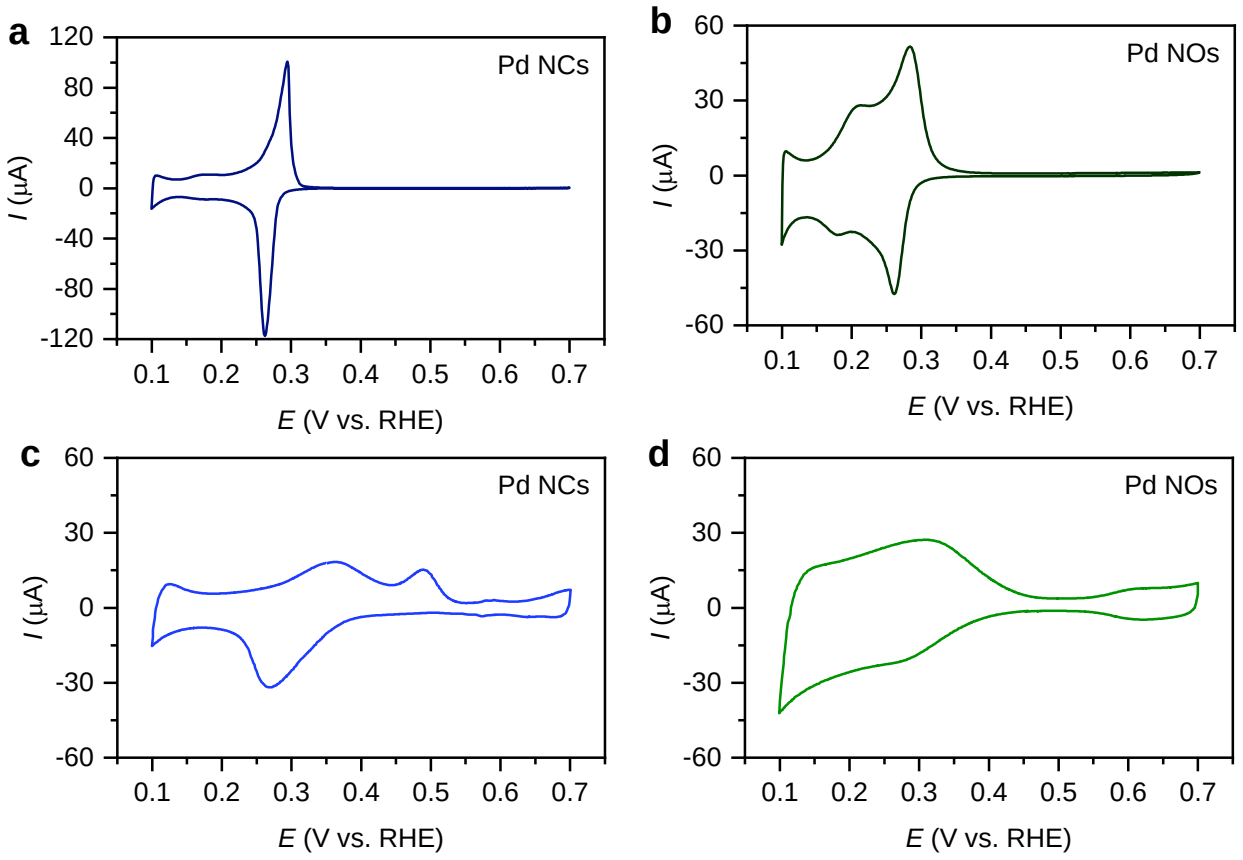
a
Pd NCs
I (μA)
E (V vs. RHE)
b
Pd NOs
I (μA)
E (V vs. RHE)
c
Pd NCs
I (μA)
E (V vs. RHE)
d
Pd NOs
I (μA)
E (V vs. RHE)

Figure 2

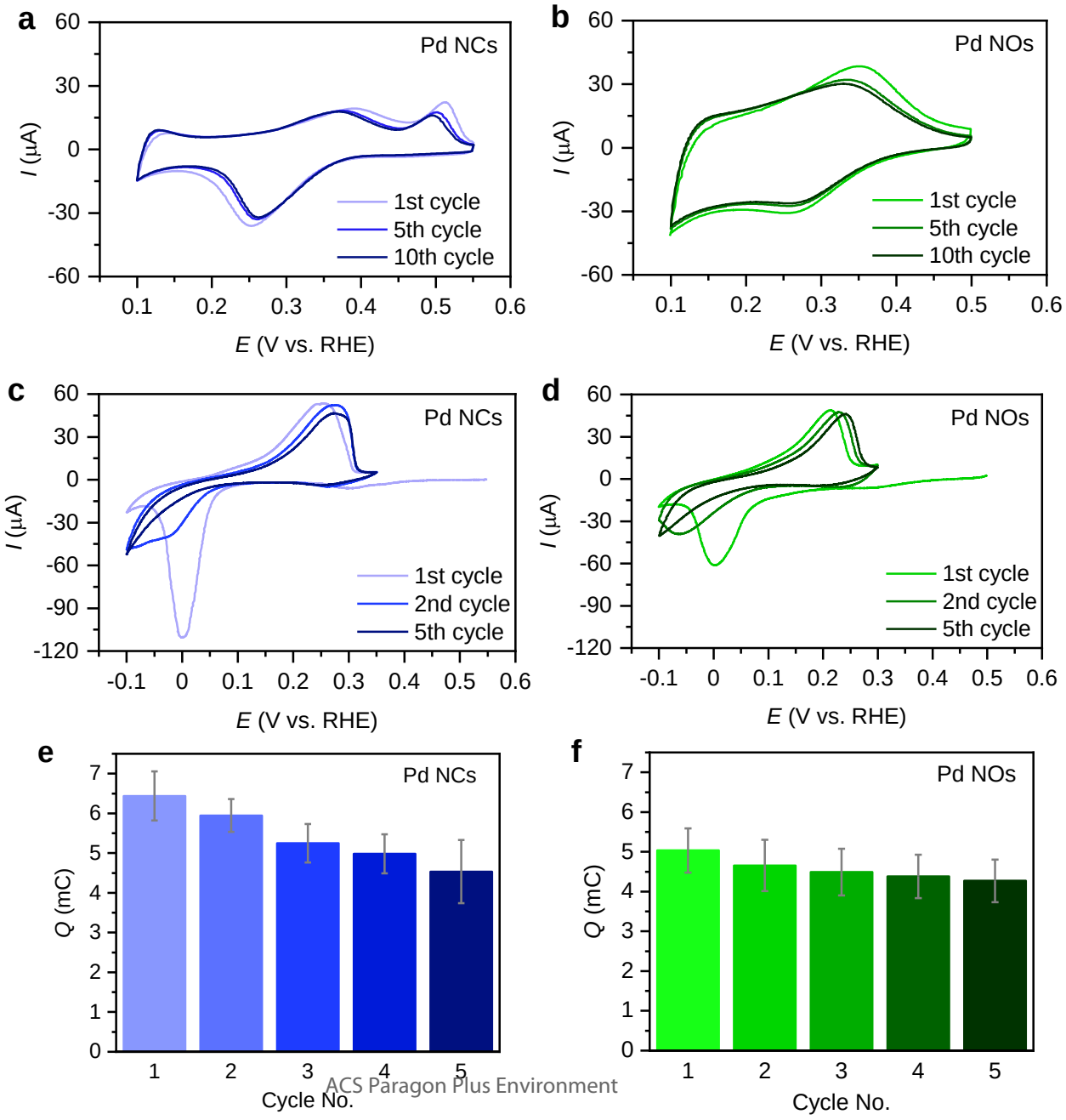

Figure 3

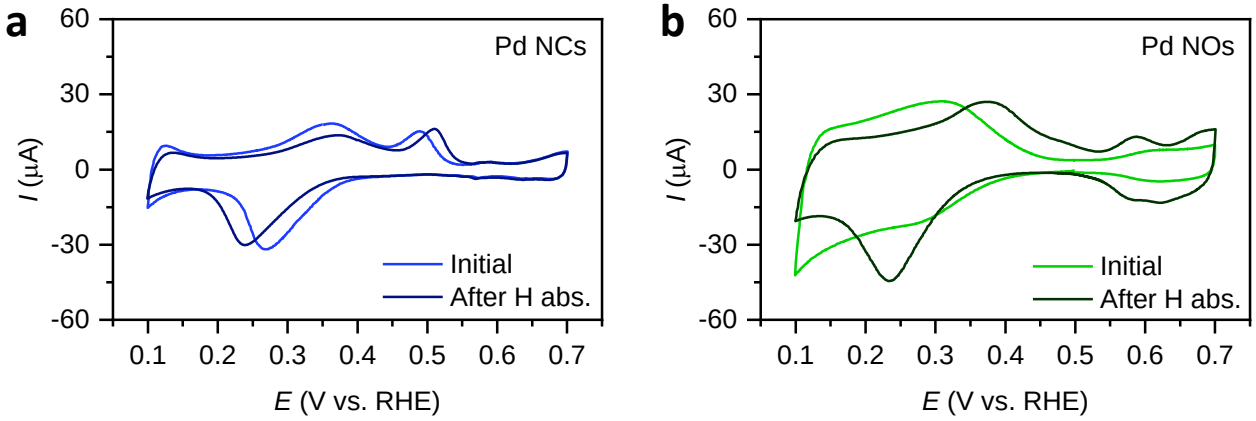
a
Pd NCs
Initial
After H abs.
I (μA)
E (V vs. RHE)
b
Pd NOs
Initial
After H abs.
I (μA)
E (V vs. RHE)

Figure 4

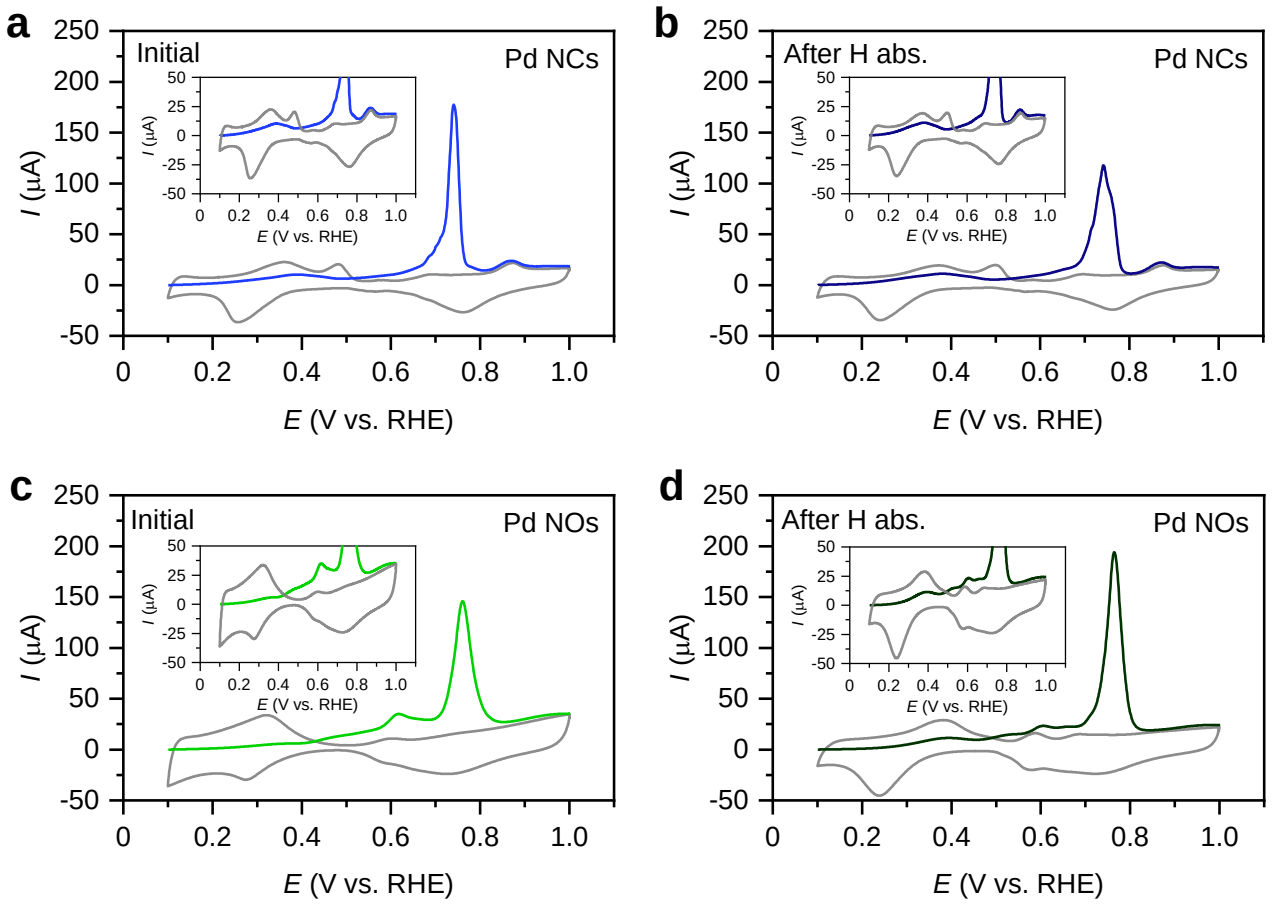
a
Initial
Pd NCs
b
After H abs.
Pd NCs
c
Initial
Pd NOs
d
After H abs.
Pd NOs
I (μA)
E (V vs. RHE)

Figure 5

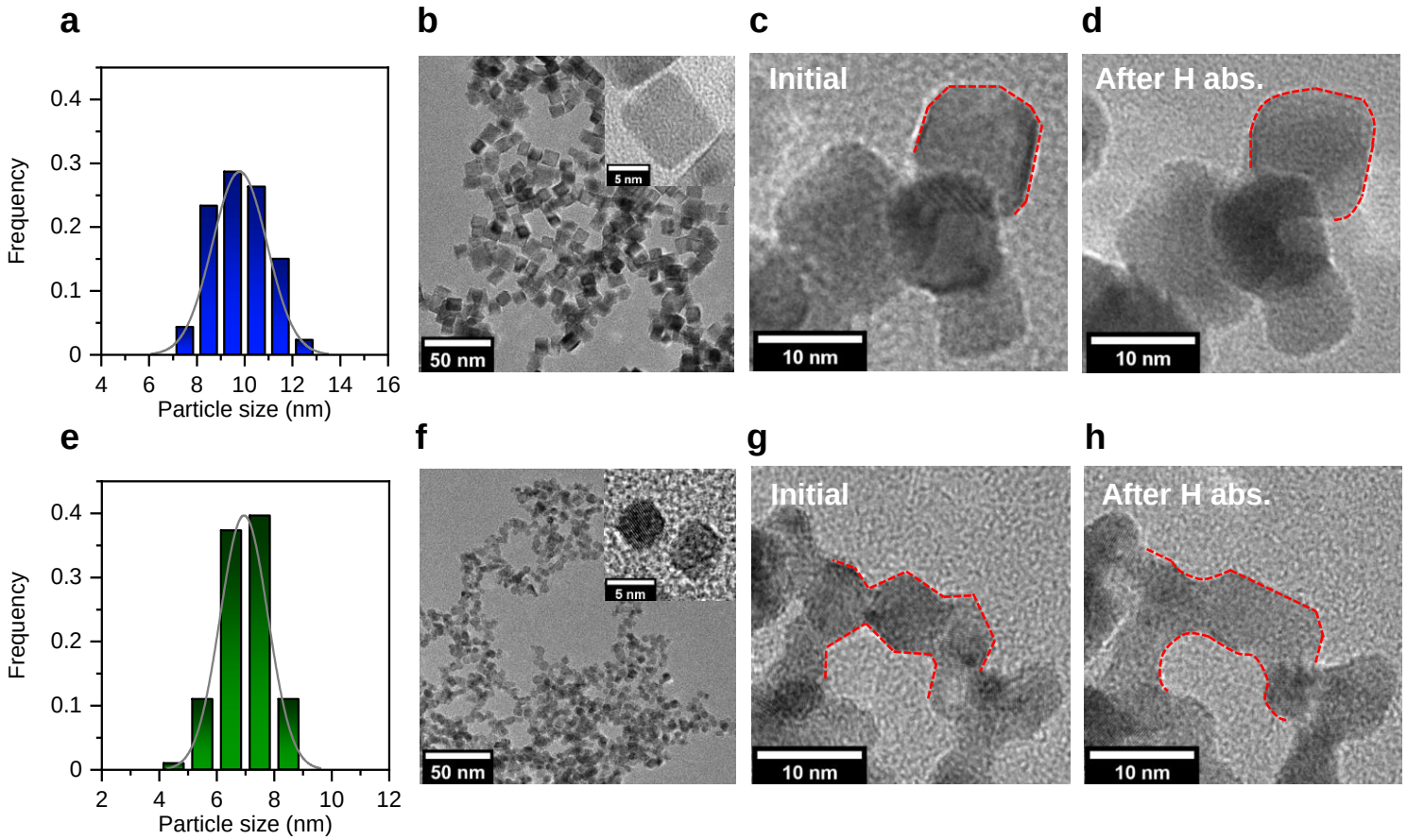
a
b
c
d
Frequency
Particle size (nm)
0.4
0.3
0.2
0.1
0
4
6
8
10
12
14
16
5 nm
50 nm
Initial
After H abs.
10 nm
e
f
g
h
2
4
6
8
10
12

Figure 6

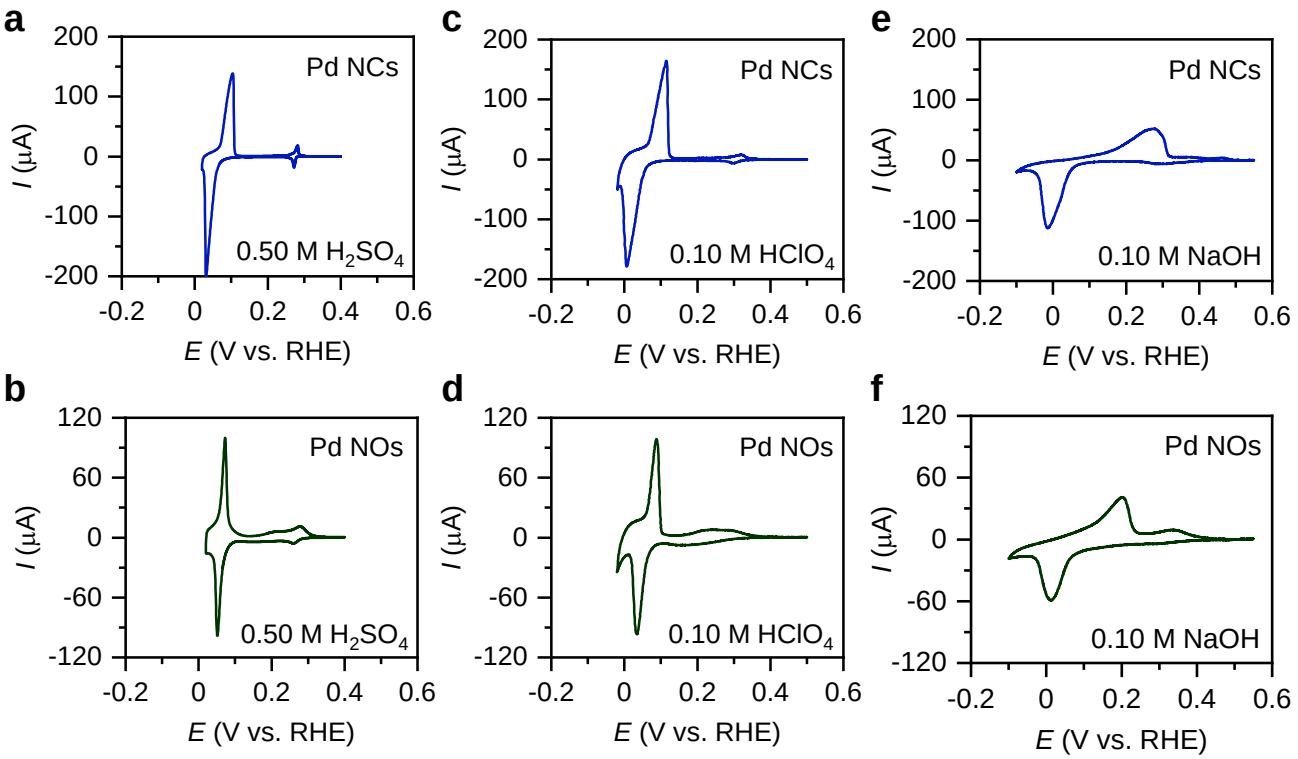
a
Pd NCs
0.50 M H2SO4
I (μA)
E (V vs. RHE)
c
Pd NCs
0.10 M HClO4
I (μA)
E (V vs. RHE)
e
Pd NCs
0.10 M NaOH
I (μA)
E (V vs. RHE)
b
Pd NOs
0.50 M H2SO4
I (μA)
E (V vs. RHE)
d
Pd NOs
0.10 M HClO4
I (μA)
E (V vs. RHE)
f
Pd NOs
0.10 M NaOH
I (μA)
E (V vs. RHE)

Figure 7

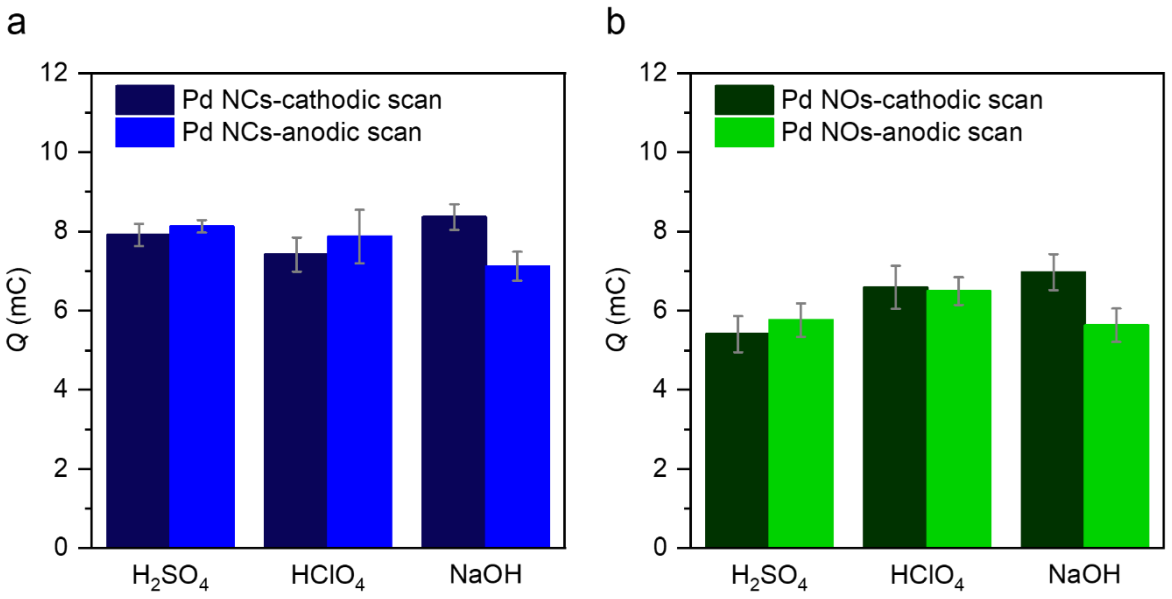
a
b
Q (mC)
Pd NCs-cathodic scan
Pd NCs-anodic scan
Pd NOs-cathodic scan
Pd NOs-anodic scan
H_2SO_4
$HClO_4$
NaOH
0
2
4
6
8
10
12

Figure 8